Research Article

Tamer Koralay* and Demet Banu Koralay

Geochemical properties and heavy metal contents of carbonaceous rocks in the Pliocene siliciclastic rock sequence from southeastern Denizli-Turkey

https://doi.org/10.1515/geo-2022-0431
received June 27, 2022; accepted October 14, 2022

Abstract: Pliocene-aged carbonaceous rocks of varying thicknesses, alternating with siliciclastic and carbonate rock units, are located on the northern border of the Çameli-Acıpayam basin (in southwestern Turkey), which is filled with thick Neogene sediments. Organic and inorganic geochemical properties of carbonaceous rocks were examined to evaluate their hydrocarbon production potential and paleo-depositional conditions (provenance, paleoclimate, paleosalinity, paleoredox, weathering, heavy metal contents, etc.). Based on organic geochemical analysis, carbonaceous rocks show good to excellent source rock potential and have gas production potential. Organic substances are mostly of allochthonous origin, and their thermal maturity degree is quite low. Carbonaceous rocks have a high amount of inorganic substance (minerals) composed of quartz, clay + mica minerals (mostly illite and a lesser amount of smectite, chlorite, and kaolinite), feldspar, and opaque minerals (pyrite and ilmenite). Although carbonaceous rocks have similar major oxide and trace element concentrations, they show clear differences in terms of Fe_2O_3, MgO, and some heavy metals (such as Ni, Cr, Co, V, and Sc). The major oxide, trace element concentrations, various element ratios of carbonaceous rocks bear the characteristics of mafic/ultramafic magmatic rocks formed on the active continental margin. In addition, carbonaceous rocks were precipitated in a brackish water environment under oxic conditions. The sediments, which were rapidly stored without recycling in the deposition environment where hot/humid climatic conditions are effective, did not undergo intense decomposition in the source area.

Keywords: carbonaceous rocks, depositional condition, provenance, paleoclimate, weathering, heavy metals

1 Introduction

Carbonaceous rocks are a type of sedimentary rocks containing significant enrichment in organic matter over average sediments (most sediments comprise a small amount of organic matter as follows: 2% mudstone, 0.3% limestone, and 0.05% sandstone) [1]. Coal, bituminous shale, clayey coal, coaly claystone, peat, and other sediments, which contain total organic carbon (TOC) content ranging from 6 to 40% are generally referred to as carbonaceous rocks. The abovementioned carbonaceous rock types are mostly used synonymously in the literature and there is no clear distinction between them [2,3]. Organic substances in carbonaceous rocks have a wide variety as they are derived from the disintegration of many plant (herbaceous, tree, and fern) and animal organisms. Inorganic substances of carbonaceous rocks are divided into detrital and authigenic origin. Detrital components are represented by rock/mineral particles that are transported to depositional environment by wind, river, and glacier effects and are directly related to the rock lithologies of the source area. On the other hand, authigenic components are characterized by new minerals formed during and/or after deposition processes [1–3].

There are numerous scientific papers related to the petrographic and geochemical properties of the organic components of carbonaceous rocks in the last 50 decades. In these studies, remarkable information was obtained about the organic matter types, amounts, compositions, maturation degrees, and hydrocarbon potentials of the carbonaceous rocks in different regions [4–15]. Although

* **Corresponding author: Tamer Koralay,** Geological Engineering Department, Faculty of Engineering, Pamukkale University, Kinikli Campus, 20017, Denizli, Turkey, e-mail: tkoralay@pau.edu.tr
Demet Banu Koralay: Geological Engineering Department, Faculty of Engineering, Pamukkale University, Kinikli Campus, 20017, Denizli, Turkey

carbonaceous rocks contain more than 100 minerals and almost all elements, research on the elemental characterization of carbonaceous rocks and their depositional conditions are limited in the literature. By using instrumental analysis techniques developed in the last few decades, inorganic components in carbonaceous rocks have become easily detectable. The investigations on organic components and results obtained from inorganic components are assessed together, and significant information (geochemical characteristic, provenance, paleoclimate, paleoredox, weathering, tectonic setting, etc.) about conditions of the deposition environment is available [16–27].

On the other hand, the share of carbonaceous rocks in electricity production in the world is 41.5%, while this ratio is 29% in Turkey, and carbonaceous rocks still constitute one of the critical energy sources in the world. Carbonaceous rocks have an important potential to cause environmental pollution according to their heavy metal content. It is known that when the limit values determined by international organizations are exceeded, heavy metal concentrations can cause serious health problems. Therefore, it is important to determine and evaluate the existing heavy metal contents of carbonaceous rocks [28–33].

The main aim of the present study is to comprehend the depositional conditions of carbonaceous rocks in Pliocene siliciclastic rock sequence from the southeast of Denizli (SW Anatolia-Turkey) based on their mineralogical, and organic-inorganic geochemical characteristics. Additionally, this study also presents data about heavy metal concentrations in the carbonaceous rocks. No similar research has been conducted in the region before. This is the first research on the provenance, paleoclimate, paleosalinity, paleoredox conditions, and weathering degree of carbonaceous rocks and its subject has been simplified to be quite understandable.

2 Field characteristics of carbonaceous rocks

Carbonaceous rocks were studied from the Yeşilyuva-Yüreğil region, about 50 km southeast of Denizli in western Turkey (Figure 1). The stratigraphy of the Yeşilyuva-Yüreğil region can be summarized as follows. The Mesozoic aged carbonate rocks (Çatalca Tepe limestone and Büyüksivri Tepe limestone), upper Jurassic-lower Cretaceous aged ophiolitic rocks (Honaz ophiolite), and lower Cretaceous-lower Eocene aged Karatepe Mélange are found at the basement of the study area. Boundaries between the basement rocks are tectonic and have a very fractured and crushed structure. All these formations at the basement are overlain with unconformity by Oligocene aged Bayıralan formation, middle-upper Miocene Kızılburun formation, Pliocene aged Yatağan formation, and Denizli volcanics, respectively. The boundaries between the Bayıralan, Kızılburun, and Yatağan formations are transitive. Oligocene aged Bayıralan formation is composed of conglomerate, sandstone, siltstone, and mudstone derived from ophiolitic origin. Kızılburun formation is represented by the conglomerate, sandstone, siltstone, and claystone. Pliocene aged Yatağan formation consists of two lithologies (siliciclastic dominant and carbonate dominant rock units). Siliciclastic rock sequence is characterized by the conglomerate, sandstone, siltstone, and claystone. The carbonate rock sequence consists of limestone, clayey limestone, marl, and claystone. Carbonaceous rocks (bituminous shale, coal, clayey coal, coaly claystone, etc.) are observed at different thicknesses inside both the lithologies of Yatağan formation (Figure 1). Denizli volcanics consist mainly of phonolite tephrite, basaltic trachyandesite, and trachyandesite. All the units in the investigated area are overlain with an unconformity by Quaternary alluvium deposits [34–41].

During the field investigations, seven different carbonaceous rock localities were determined. Carbonaceous rocks were bedded/laminated or lens-shaped formations at a variable thickness (<3–15 cm) among claystone, sandstone, and conglomerate alternations. While systematic sampling was carried out along the measured stratigraphic section (MSS) in localities 1 and 3, point samples were collected from other localities (nos. 2, 4, 5, 6, and 7) because the outcrops were covered. A detailed MSS belonging to locality 1 is presented in Figure 2. Fresh surfaces of carbonaceous rocks are black, grayish black, brownish black to reddish brown in color and characteristically show cleat fractures on the bedding surfaces (Figure 3a and b). Oxidation surfaces in yellowish orange color are common in laminated structure carbonaceous rocks (Figure 3c). Partially preserved gastropod shells and wood chips can be identified in bedded carbonaceous rocks (thickness of 10–15 cm) (Figure 3d and e). The lens-shaped carbonaceous rocks are generally brown in color, have an earthy structure, and contain abundant plant roots (Figure 3f).

3 Analytical techniques

TOC and Rock-Eval pyrolysis analyses were performed to determine the organic geochemical properties of a total of

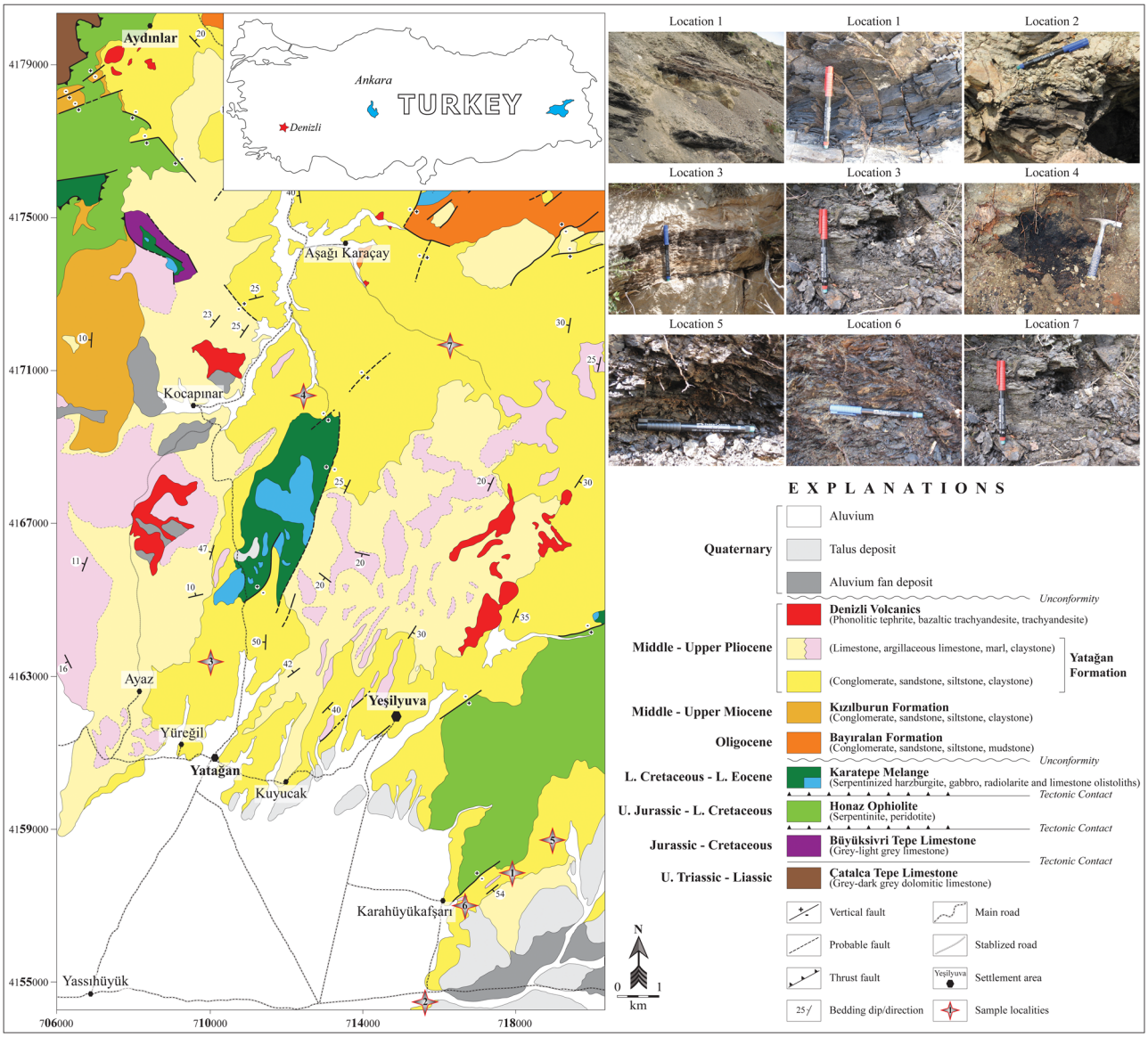

Figure 1: Geographic position, geologic map (modified from [35]), and field views of carbonaceous rocks.

21 carbonaceous samples. The sampling strategy has been given in detail in ref. [15]. These analyses were carried out at Applied Petroleum Technology AS (Norway). Leco SC-632 device is used for TOC measurement. Diluted HCl is added to the crushed rock sample to remove carbonate. The sample is then introduced into the Leco combustion oven, and the amount of carbon in the sample is measured as carbon dioxide by an IR-detector. A HAWK device is used for Rock-Eval pyrolysis analysis. Jet-Rock 1 was run for every ten samples and the measurements were checked according to NIGOGA standards.

To identify the mineral matter components and clay mineral compositions of the carbonaceous rock samples, a Rigaku D/Max-2200 Powder X-ray Diffractometer (XRD) was used. For the whole rock XRD analyses, four carbonaceous rock samples were crushed in a tungsten carbide crushing vessel. After that, samples were subjected to 3 different XRD clay mineral analyses by saturating them with ethylene glycol vapor for 8 h and firing at 550°C for 2.5 h. X-ray diffraction patterns were obtained with a 40 kV and 20 mA X-ray detector consisting of a copper anode ($\lambda = 1.54059$ Å). The diffracted radiation was obtained between 0° and 70°, with an acquisition time of 60 s/step for whole rock and 30 s/step for clay analysis.

Major oxides and trace elements including rare earth elements were analyzed by using ICP-ES/MS at the ACME Laboratories in Canada. For analyses, 21 carbonaceous rock samples were crushed in a tungsten carbide crushing

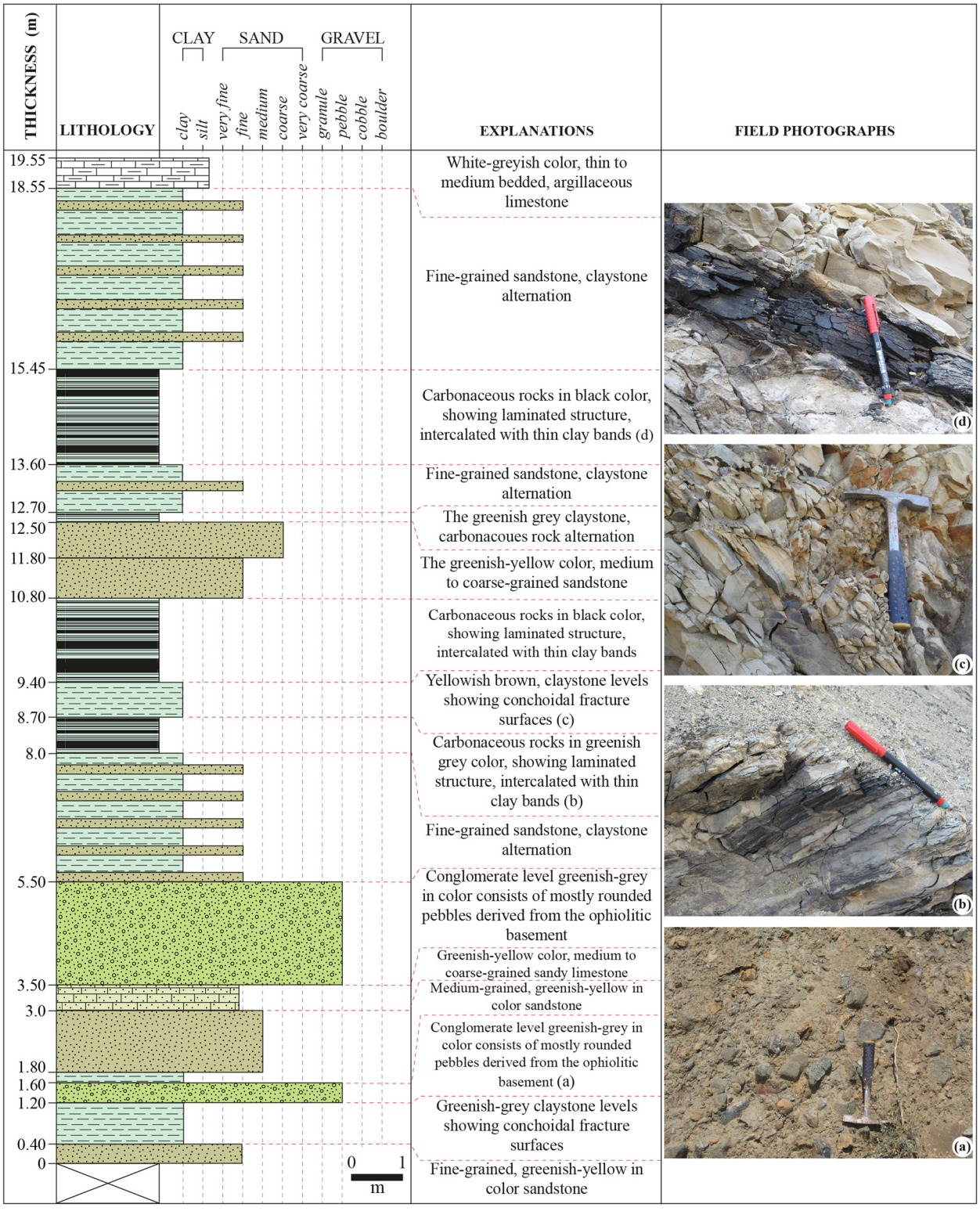

Figure 2: MSS and field photographs of carbonaceous rocks in locality 1.

Figure 3: (a) Carbonaceous rocks with a layered structure in siliciclastic rock sequence. (b) Cleat structures typically seen in carbonaceous rocks. (c) Yellowish orange oxidation surfaces on bedding surfaces. (d and e) Partially preserved gastropod shells and wood chips. (f) Close view of lens-shaped carbonaceous rocks.

vessel and pulverized to 85% passing 200 meshes. After that, the 0.5 g powdered sample and 1.5 g $LiBO_2$ were melted in an oven under 1050°C temperature, and the melt was then added to 100 mL, 5% HNO_3.

4 Organic geochemical properties

Totally 21 carbonaceous rock samples have been analyzed by the TOC/Rock-Eval method and results are presented in Table 1. Organic geochemical parameters derived from the TOC/Rock-Eval analyses of carbonaceous rocks have been evaluated based on the quantity (richness), quality (types of organic matter), and thermal maturity of organic matter. The plots of hydrogen index (HI) vs T_{max}, HI vs TOC, HI vs S2/S3, and finally S2 vs TOC diagrams are useful in evaluating the hydrocarbon generative potential and organic matter type of source rocks [42–45]. These diagrams classify carbonaceous rocks as containing mainly type III, gas prone organic matter and very good–excellent source rock potential (Figure 4a–d). The thermal maturity of the organic matter rich samples was evaluated by production index (PI) vs T_{max} diagram. Carbonaceous rocks have immature character in this diagram (Figure 4d). S1 and S2 values for the studied rocks are high. The high S1 (0.12–4.0 mg HC/g rock) and S2 (0.37–63.41 mg HC/g rock) and low HI (12–171 mg HC/g TOC) and T_{max} values (390–440°C) for the carbonaceous rocks may indicate presence of pre and syn-depositional organic matter degradation [46].

Table 1: TOC/Rock-Eval pyrolysis results of carbonaceous rocks

Localities	Sample code	TOC (%)	S_1	S_2	S_3	T_{max} (°C)	PY	PI	HI	OI	S_2/S_3	S_1/TOC
1	KHA-3	36.60	1.80	37.57	21.33	420	39.37	0.05	103	58	1.76	0.05
	KHA-4	43.80	1.73	47.69	25.05	433	49.42	0.04	109	57	1.90	0.04
	KHA-6	13.20	0.52	5.67	8.89	425	6.19	0.08	43	67	0.64	0.04
	KHA-8	39.00	2.89	57.40	20.29	410	60.29	0.05	147	52	2.83	0.07
	KHA-9	37.00	3.92	63.41	33.31	428	67.33	0.06	171	90	1.90	0.11
	KHA-10	21.40	1.42	18.43	7.69	415	19.85	0.07	86	36	2.40	0.07
	KHA-12	19.00	1.28	19.75	10.01	427	21.03	0.06	104	53	1.97	0.07
	KHA-14	8.82	0.55	7.38	3.72	421	7.93	0.07	84	42	1.98	0.06
	KHA-15	40.30	4.00	46.38	16.52	421	50.38	0.08	115	41	2.81	0.10
	KHA-16	32.00	2.64	40.76	21.84	421	43.40	0.06	127	68	1.87	0.08
	KHA-21	38.90	3.67	55.11	25.62	411	58.78	0.06	142	66	2.15	0.09
2	MD-1	20.60	1.06	18.79	8.23	420	19.85	0.05	91	40	2.28	0.05
3	TRY 2	14.50	0.62	5.13	10.97	400	5.75	0.11	35	76	0.47	0.04
	TRY 3	18.70	1.67	9.67	15.83	390	11.34	0.15	52	85	0.61	0.09
	TRY 5	10.60	0.46	7.12	8.02	429	7.58	0.06	67	76	0.89	0.04
	YRG 3	3.01	0.12	0.37	2.12	434	0.49	0.24	12	70	0.17	0.04
4	KRÇ-2	5.02	0.41	1.92	1.94	440	2.33	0.18	38	39	0.99	0.08
5	KKLP-2	16.8	1,38	11.79	10.2	435	13.17	0,1	70	61	1,16	0,08
	KKLP-3	17.7	1	11.4	8.69	428	12.4	0.08	64	49	1,31	0,06
6	KINC-2	25.3	3.56	30.16	15.45	427	33.72	0.11	119	61	1.95	0.14
7	BDR-1	8.58	0.73	7.74	1.52	401	8.47	0.09	90	18	5.09	0.09

TOC: total organic carbon (wt%); **S1:** volatile hydrocarbon (HC) content, mg HC/g rock; **S2:** remaining HC generative potential, mg HC/g rock; **S3:** carbon dioxide yield, mg CO2/g rock; **HI:** hydrogen index = S2 100/TOC, mg HC/g rock; **OI:** oxygen index = S3 100/TOC, mg CO_2/g TOC; **PI:** production index = S1/(S1 + S2); **PY:** potential yield = S1 + S2; T_{max}: temperature at maximum generation.

On the other hand, the plot of S1 vs TOC can be used to discriminate between allochthonous (non-indigenous) and autochthonous (indigenous) organic matter. The carbonaceous rock samples fall into the allochthonous area in the diagram (Figure 4e).

5 Mineral contents of carbonaceous rocks

According to whole rock XRD analysis, carbonaceous rocks are chiefly composed of quartz, clay and mica minerals, feldspar, opaque minerals, and a lesser amount of calcite and gypsum. The main opaque minerals were mainly pyrite with a minor quantity of ilmenite. In addition, carbonaceous rocks have partially complex XRD patterns because of clay mineral contents. The dominant clay mineral in carbonaceous rocks is illite which is formed by the weathering of Fe, Mg-rich silicates (olivine, pyroxene, amphibole, etc.), alteration of other clay minerals, and muscovite. Furthermore, smectite, mixed layer illite/smectite, kaolinite, and chlorite peaks were detected in clay fraction X-ray diffractograms, respectively [15].

6 Geochemical characteristic of carbonaceous rocks

The source of elements in carbonaceous rocks can be related to siliciclastic materials carried by water to the sedimentation environment, organic matter, atmospheric dust (volcanic ash and cosmic dust), epigenetic mineralization, and solutions [2]. On the other hand, the inorganic/mineral components of sedimentary rocks are directly related to the mineralogical and petrographic properties of the basement rocks in their region. The major, trace, and rare earch element's (REE) composition of the carbonaceous rocks are presented in Table 2. Major oxide compositions of carbonaceous rocks are as follows: SiO_2 from 3.32 to 47.16 wt%, TiO_2 from 0.05 to 0.75 wt%, Al_2O_3 from 0.91 to 12.72 wt%, Fe_2O_3 (as total iron) from 0.99 to 10.49 wt%, MgO from 2.40 to 19.96 wt%, CaO from 0.31 to 1.44 wt%, Na_2O from 0.02 to 0.66 wt%, and K_2O from 0.08 to 2.20 wt%. The major oxide values for all localities are shown in the box-plot diagrams (Figure 5). While all localities display similar compositional distribution in terms of CaO, NaO_2, and K_2O contents, they vary in terms of SiO_2, TiO_2, Al_2O_3, Fe_2O_3, and MgO contents. This can be explained that the terrestrial clastic materials

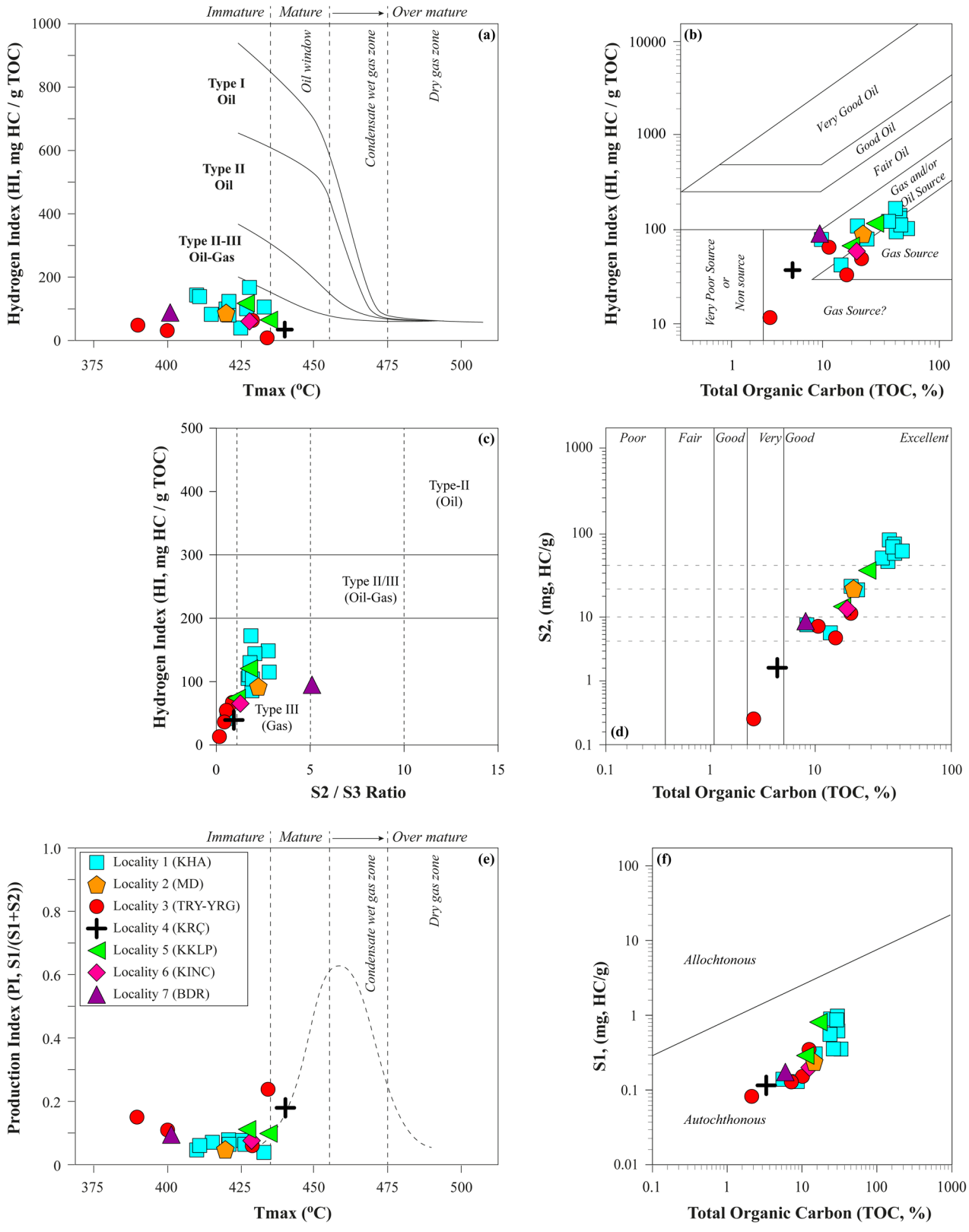

Figure 4: Organic geochemical diagrams for characterization of carbonaceous rocks: (a) HI vs T_{max}, (b) HI vs TOC, (c) HI vs S2/S3, (d) S2 vs TOC, (e) PI vs T_{max}, and (f) S1 vs TOC diagrams.

transported to the depositional environment of carbonaceous rocks are of various origins and amounts.

All carbonaceous rock samples have slight differences and limited compositional spread in terms of trace elements (Figure 5). They have a higher content of Ni (average 1956.9 ppm), Cr (average 934.3 ppm), Co (average 101.1 ppm), and V (average 107.5 ppm) elements than other trace elements. The Post Archean Australian Shale (PAAS; [47]), the North American Shale Composition (NASC; [48]), and the Average Shale Composition (ASC; [49]) normalized trace element patterns of the carbonaceous rock samples are shown in Figure 6a–c. It is clear from Figure 6a–c that the carbonaceous rocks display slight depletions in trace element contents. Depletions in trace elements reflect

Table 2: Major oxide (wt%), trace (ppm), and REE analyses results of carbonaceous rocks

Localities	Sample code	SiO_2 wt%	Al_2O_3 wt%	Fe_2O_3 wt%	MgO wt%	CaO wt%	Na_2O wt%	K_2O wt%	TiO_2 wt%	P_2O_5 wt%	MnO wt%	LOI* wt%	Total wt%
1	KHA-3	9.11	1.81	2.84	5.42	1.22	0.09	0.11	0.09	0.01	—	78.60	99.30
	KHA-4	3.32	0.91	0.99	4.09	1.44	0.05	0.08	0.05	—	—	88.20	99.13
	KHA-6	33.58	4.70	6.51	13.09	0.80	0.15	0.16	0.18	—	0.03	40.00	99.20
	KHA-8	10.70	1.63	2.21	4.53	0.91	0.07	0.10	0.08	—	—	79.30	99.53
	KHA-9	9.17	1.92	2.00	5.04	1.26	0.08	0.10	0.09	—	—	79.90	99.56
	KHA-10	27.68	4.41	5.72	9.76	0.73	0.17	0.17	0.18	0.01	0.02	50.40	99.25
	KHA-12	29.49	2.66	4.65	15.14	0.75	0.16	0.13	0.15	0.02	0.03	46.10	99.28
	KHA-14	41.10	3.16	6.09	19.96	0.64	0.21	0.11	0.17	0.02	0.03	27.60	99.09
	KHA-15	10.17	2.08	3.15	3.49	0.76	0.09	0.14	0.10	0.01	—	79.70	99.69
	KHA-16	17.19	2.44	6.42	4.29	0.56	0.09	0.20	0.11	—	—	68.30	99.60
	KHA-21	10.12	1.46	2.32	3.81	1.18	0.09	0.12	0.08	0.01	—	80.30	99.49
2	MD-1	27.45	4.60	5.43	13.28	1.14	0.07	0.36	0.24	0.02	0.03	46.70	99.32
3	TRY-2	33.86	6.69	9.22	4.98	0.54	0.04	0.37	0.36	0.03	0.03	43.50	99.62
	TRY-3	24.44	5.49	7.53	4.25	0.31	0.02	0.33	0.26	0.02	0.03	57.00	99.68
	YRG-3	45.77	9.50	10.49	6.49	1.31	0.05	0.49	0.50	0.02	0.04	24.80	99.46
4	KRC-2	47.16	10.29	8.47	6.30	0.79	0.04	0.49	0.58	0.02	0.03	25.30	99.47
5	KKLP-2	25.05	4.52	5.67	8.48	0.60	0.03	0.34	0.21	—	0.01	54.30	99.21
	KKLP-3	28.81	5.41	6.43	8.20	0.64	0.05	0.48	0.27	—	0.02	48.90	99.21
6	KINC-2	24.31	4.24	9.18	3.74	0.94	0.14	0.37	0.21	—	0.02	56.40	99.55
7	BDR-1	46.38	12.72	9.45	2.40	0.63	0.66	2.20	0.75	0.06	0.03	24.40	99.68

Localities	Sample code	Ni ppm	Cr ppm	Sc ppm	Ba ppm	Co ppm	Cs ppm	Ga ppm	Hf ppm	Nb ppm	Rb ppm	Sr ppm	Zr ppm
1	KHA-3	2859.3	1361.6	5.0	22.0	182.0	1.4	2.8	0.5	1.4	5.4	72.8	15.7
	KHA-4	479.3	225.8	2.0	15.0	24.6	0.4		0.3	1.1	3.4	76.6	11.4
	KHA-6	3132.8	855.3	17.0	29.0	138.3	2.0	5.7	0.6	2.2	9.9	34.1	22.9
	KHA-8	1993.3	725.3	5.0	20.0	61.6	1.1	2.5	0.4	1.2	5.6	41.3	14.9
	KHA-9	2005.0	355.8	6.0	21.0	99.2	1.2	2.8	0.4	1.7	5.2	56.8	15.6
	KHA-10	3097.9	998.9	16.0	35.0	167.5	2.1	5.9	0.7	2.1	10.1	27.4	25.0
	KHA-12	2291.9	1361.6	9.0	22.0	104.3	1.8	4.1	0.5	1.7	7.5	27.9	18.4
	KHA-14	2452.9	1525.8	12.0	23.0	122.1	1.4	4.2	0.6	1.6	5.8	18.2	22.1
	KHA-15	1365.0	478.9	5.0	27.0	38.8	1.9	2.8	0.5	1.8	7.7	31.5	17.8
	KHA-16	1501.4	451.6	7.0	27.0	65.7	3.9	3.3	0.7	2.0	12.6	28.9	20.4
	KHA-21	2951.3	424.2	4.0	21.0	123.0	1.8	2.3	0.4	1.6	6.2	63.2	15.4
2	MD-1	2015.0	1341.0	11.0	48.0	165.7	3.9	5.2	1.2	7.3	20.8	31.3	53.6
3	TRY-2	1247.7	773.1	16.0	60.0	90.1	6.0	8.4	1.3	6.2	28.6	34.2	55.8
	TRY-3	1156.6	492.6	13.0	41.0	84.4	4.2	6.1	0.9	4.5	24.2	26.7	38.0
	YRG-3	1475.0	1176.8	23.0	88.0	143.1	7.1	10.2	1.8	8.2	37.5	51.5	72.1
4	KRC-2	900.6	1341.0	16.0	98.0	55.3	1.7	11.7	2.5	11.4	20.6	47.3	101.1
5	KKLP-2	3599.4	1190.5	15.0	32.0	140.2	3.8	4.4	1.3	5.5	21.6	46.5	58.5
	KKLP-3	2918.0	1922.6	14.0	45.0	131.1	5.7	4.6	1.5	6.2	28.8	37.8	71.5
6	KINC-2	1311.9	738.9	11.0	47.0	54.0	44.9	3.2	1.0	3.1	41.3	58.5	36.4
7	BDR-1	383.4	944.2	15.0	375.0	31.6	6.9	14.8	6.0	16.1	97.5	86.3	225.2

(*Continued*)

Table 2: *Continued*

Localities	sample code	Th ppm	U ppm	V ppm	Y ppm	Mo ppm	Cu ppm	Pb ppm	Zn ppm	Cd ppm	Hg ppm	Se ppm
1	KHA-3	0.9	0.3	224.0	13.7	2.3	21.8	1.4	41.0	0.1	0.06	6.6
	KHA-4	0.7	0.3	69.0	6.6	0.8	6.4	1.1	18.0		0.04	1.5
	KHA-6	1.6	0.3	66.0	3.9		29.6	2.0	50.0	0.1	0.03	1.6
	KHA-8	0.9	0.3	102.0	7.4	1.9	17.9	1.4	21.0	0.1	0.03	5.7
	KHA-9	1.1	0.3	68.0	8.1	1.7	13.7	1.3	14.0	—	0.04	1.7
	KHA-10	1.6	0.4	75.0	4.8	0.8	29.3	2.1	41.0	—	0.04	0.7
	KHA-12	1.0	0.2	71.0	3.9	0.5	26.3	1.4	32.0	—	0.03	1.6
	KHA-14	0.9	0.3	71.0	2.7	0.5	24.2	1.4	41.0	0.1	0.02	0.9
	KHA-15	1.2	0.4	62.0	7.3	3.1	13.1	1.7	17.0	0.1	0.05	1.8
	KHA-16	1.4	0.6	59.0	5.8	3.3	17.2	2.4	29.0	—	0.04	2.0
	KHA-21	0.9	0.2	50.0	3.4	1.7	17.4	1.6	25.0	0.1	0.06	2.1
2	MD-1	4.6	1.7	126.0	20.1	2.8	25.0	5.7	46.0	0.2	0.03	2.6
3	TRY-2	3.0	17.8	89.0	9.8	18.3	54.6	4.1	58.0	0.2	0.04	3.0
	TRY-3	2.6	22.3	89.0	10.8	14.4	54.5	3.4	79.0	0.2	0.04	5.8
	YRG-3	4.0	3.6	109.0	14.6	0.7	51.7	5.4	94.0	0.2	0.03	0.9
4	KRC-2	6.3	1.0	183.0	17.8	—	36.7	9.7	45.0	0.1	0.07	0.9
5	KKLP-2	4.5	0.5	196.0	17.0	0.2	24.6	4.2	45.0	0.2	0.05	8.2
	KKLP-3	4.3	1.6	214.0	19.3	0.8	37.5	5.2	47.0	0.3	0.04	10.9
6	KINC-2	2.0	5.2	96.0	10.6	7.6	35.9	3.0	30.0	0.1	0.04	3.7
7	BDR-1	11.6	9.2	131.0	28.5	14.9	29.3	15.7	50.0	0.6	0.12	1.2

Localities	Sample code	La ppm	Ce ppm	Pr ppm	Nd ppm	Sm ppm	Eu Ppm	Gd ppm	Tb ppm	Dy ppm	Ho ppm	Er ppm	Tm ppm	Yb ppm	Lu ppm
1	KHA-3	3.90	7.80	1.18	5.70	1.46	0.42	1.96	0.29	1.86	0.47	1.28	0.16	1.17	0.18
	KHA-4	4.30	8.60	1.07	4.70	0.91	0.25	1.09	0.12	0.82	0.18	0.53	0.06	0.39	0.06
	KHA-6	2.80	4.40	0.64	2.50	0.43	0.09	0.54	0.09	0.68	0.14	0.47	0.06	0.41	0.07
	KHA-8	3.10	6.00	0.89	3.80	1.01	0.30	1.11	0.19	1.13	0.23	0.81	0.11	0.68	0.10
	KHA-9	3.90	9.00	1.12	4.90	1.03	0.32	1.17	0.20	1.15	0.28	0.71	0.11	0.67	0.09
	KHA-10	3.40	6.10	0.84	3.50	0.68	0.19	0.75	0.12	0.90	0.18	0.56	0.08	0.48	0.08
	KHA-12	2.20	4.00	0.55	2.10	0.42	0.13	0.53	0.09	0.61	0.14	0.41	0.07	0.45	0.07
	KHA-14	2.40	4.00	0.52	2.00	0.34	0.10	0.54	0.08	0.55	0.11	0.37	0.05	0.35	0.05
	KHA-15	3.90	8.00	1.05	4.30	0.97	0.26	1.17	0.18	0.95	0.25	0.71	0.10	0.56	0.09
	KHA-16	3.70	7.10	0.99	3.70	0.84	0.21	0.96	0.16	0.92	0.21	0.51	0.08	0.46	0.09
	KHA-21	2.90	4.70	0.68	2.60	0.50	0.13	0.61	0.09	0.59	0.11	0.28	0.05	0.31	0.05
2	MD-1	11.70	22.60	3.02	11.30	2.42	0.65	3.22	0.48	2.72	0.60	1.74	0.25	1.53	0.26
3	TRY-2	9.30	18.20	2.31	8.60	1.99	0.53	2.05	0.30	1.83	0.37	0.98	0.14	0.98	0.15
	TRY-3	9.40	19.10	2.66	10.80	2.69	0.75	2.66	0.43	2.30	0.42	1.33	0.16	1.37	0.18
	YRG-3	13.40	26.10	3.24	12.60	2.74	0.72	2.98	0.45	2.64	0.53	1.57	0.20	1.42	0.28
4	KRC-2	21.50	41.20	4.95	19.00	3.61	0.88	3.57	0.51	3.27	0.59	1.89	0.25	1.71	0.25
5	KKLP-2	8.40	18.20	2.33	9.30	2.16	0.58	2.41	0.37	2.46	0.53	1.62	0.22	1.34	0.22
	KKLP-3	8.40	16.30	2.18	9.00	2.17	0.58	2.56	0.41	2.97	0.65	1.94	0.26	1.78	0.25
6	KINC-2	9.10	17.60	2.03	7.80	1.47	0.47	1.99	0.29	1.77	0.39	0.93	0.14	0.94	0.15
7	BDR-1	35.40	73.00	8.17	31.90	6.02	1.25	5.62	0.79	4.95	0.93	2.89	0.43	2.81	0.43

the characteristics of mafic-ultramafic rocks. In addition, the carbonaceous rocks from locality 1 are more depleted than the other localities. This can be associated with the position of locality 1 which is in a close area to the mafic/ultramafic basement rocks (Honaz Ophiolite and Karatepe Melange).

The total REE concentration of carbonaceous rocks ranges from 11.46 to 174.59 ppm (average 43.06 ppm). This value is prominently lower than the PAAS (184.77 ppm), NASC (159.13 ppm), and ASC (193.60 ppm) values and is similar to the average coal value (50.40 ppm) [47–50]. The PAAS, NASC, and ASC normalized REE pattern of carbonaceous samples are illustrated in

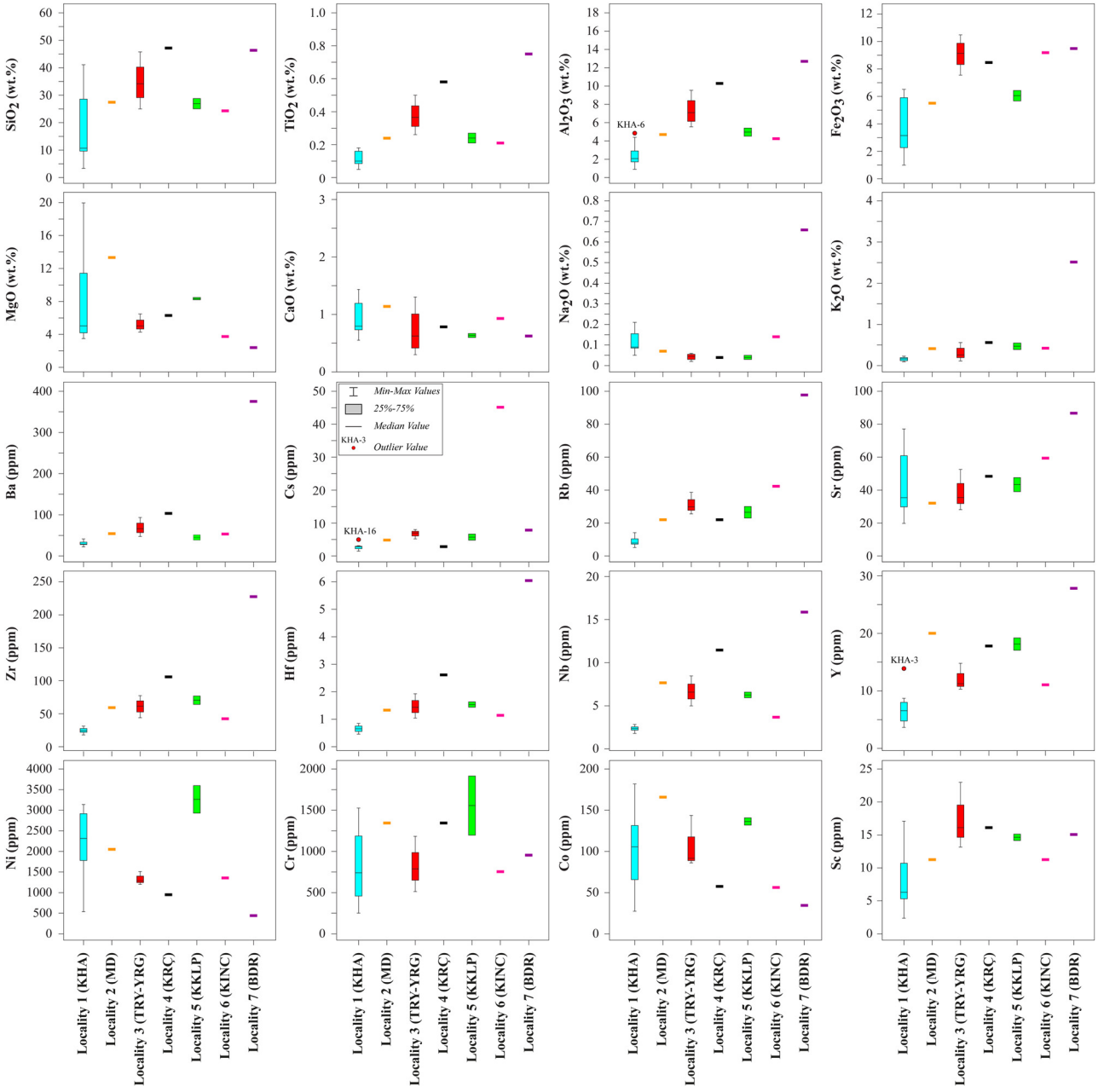

Figure 5: Selected major oxide and trace element boxplots of carbonaceous rocks from different localities.

Figure 6d–f. In PAAS, NASC, and ASC normalized REE diagrams, carbonaceous rocks show similar and flat patterns ($(La/Lu)_{PAAS}$ = 0.25–0.97; $(La/Lu)_{NASC}$ = 0.32–1.26; $(La/Lu)_{ASC}$ = 0.21–0.84). In addition, the REE patterns of carbonaceous rocks have a negligible amount of depletion in light rare earth element (LREE) ($(La/Sm)_{PAAS}$ = 0.39–1.03; $(La/Sm)_{NASC}$ = 0.51–1.36; $(La/Sm)_{ASC}$ = 0.39–1.02) relative to heavy rare earth element ($(Sm/Lu)_{PAAS}$ = 0.47–1.18; $(Sm/Lu)_{NASC}$ = 0.46–1.16; $(Sm/Lu)_{ASC}$ = 0.41–1.03). Moreover, carbonaceous rock samples have slightly positive Europium (Eu/Eu*) anomalies ($(Eu/Eu^*)_{PAAS}$ = 0.88–1.37; $(Eu/Eu^*)_{NASC}$ = 0.90–1.40; $(Eu/Eu^*)_{ASC}$ = 0.88–1.37) (Figure 6d–f). Eu enrichment is normally interpreted as the result of plagioclase enrichment, the presence of mafic detritus, or a concentration of Eu-rich phases (e.g., epidote). However, presence of such components should be supported by additional information (e.g., XRD analysis, petrography, etc.). An alternative explanation that could be considered is the diagenetic mobilization and reconcentration of Eu under anoxic conditions as the cause of the positive Eu anomaly [51].

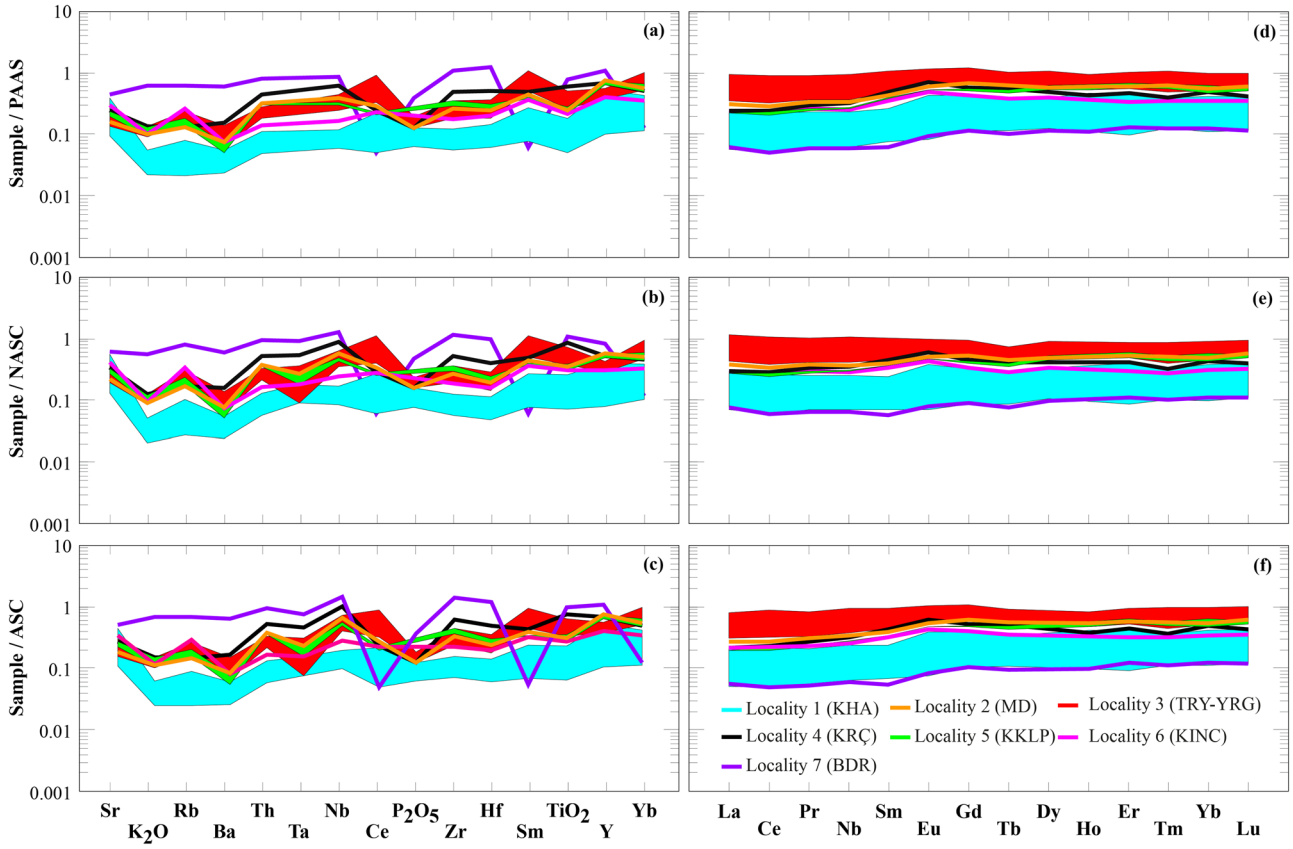

Figure 6: (a and d) PAAS normalized [47], (b and e) NASC normalized [48], and (c and f) ASC normalized [49] trace and REE patterns of carbonaceous rocks.

7 Chemical nomenclature

The detritic/authigenic index (DAI) is useful for determining whether components in sedimentary rocks are of detrital or authigenic origin. While Si, Al, K, Ti, and Na oxide elements are found in the chemical composition of detrital minerals such as quartz, feldspar, clay (except kaolinite and illite) and mica minerals, volcanic glass, Al oxide/hydroxide, rutile-anatase-brookite, Fe, Ca, Mg, S, P, and Mn oxide elements are found in the chemical composition of authigenic minerals such as Fe–Mn sulfides, Ca–Fe–Mg sulfates, Ca–Mg–Fe–Mn carbonates, and Ca–Fe phosphates [52]. The DAI values of the carbonaceous rock samples vary between 0.68 and 5.02 (average 2.12), pointing to detrital origin.

The (SiO_2 + Al_2O_3 + K_2O + TiO_2)–(CaO + MgO + SO_3 + Na_2O) – (Fe_2O_3) triangular diagram can be used to determine inorganic/mineral constituents in carbonaceous rocks [53]. While the carbonaceous rocks from 1, 2, and 5 localities are plotted in the CS field, the samples from 3, 4, and 7 localities fall in the S field. Moreover, the sample from locality 6 falls in the FS field. All carbonaceous rock samples were formed under low to moderate acidic conditions (Figure 7a).

The (Al_2O_3/TiO_2)–SiO_2(%), log(Fe_2O_3/K_2O)–log(SiO_2/Al_2O_3), and K_2O(%)-Rb (ppm) diagrams can be utilized to determine the origin of inorganic/mineral components in carbonaceous rock samples. In the (Al_2O_3/TiO_2)–SiO_2(%) diagram proposed by Le Bas et al. [54], the carbonaceous rock samples fall into the ultramafic-mafic field (Figure 7b). In the log(Fe_2O_3/K_2O)–log(SiO_2/Al_2O_3) diagram advised by Herron [55], the samples are mostly concentrated in Fe-sand and Fe-shale areas (Figure 7c). The distinction between basic and acidic-intermediate constituents can be more easily recognized by using the K_2O(%)-Rb (ppm) diagram. While the K/Rb ratio in acidic and intermediate rocks is higher than 230, it is lower than 230 in basic rocks [56]. The K/Rb ratios of the carbonaceous rocks vary between 74.4 and 197.5 (average 144.6), and the samples were mostly plotted in the basic field (Figure 7d). Considering the geological background of the region, the presence of Honaz ophiolite and Bayıralan formation consisting of ultramafic-mafic rocks support the enrichment of Ca, Mg, and Fe components in the carbonaceous rock samples.

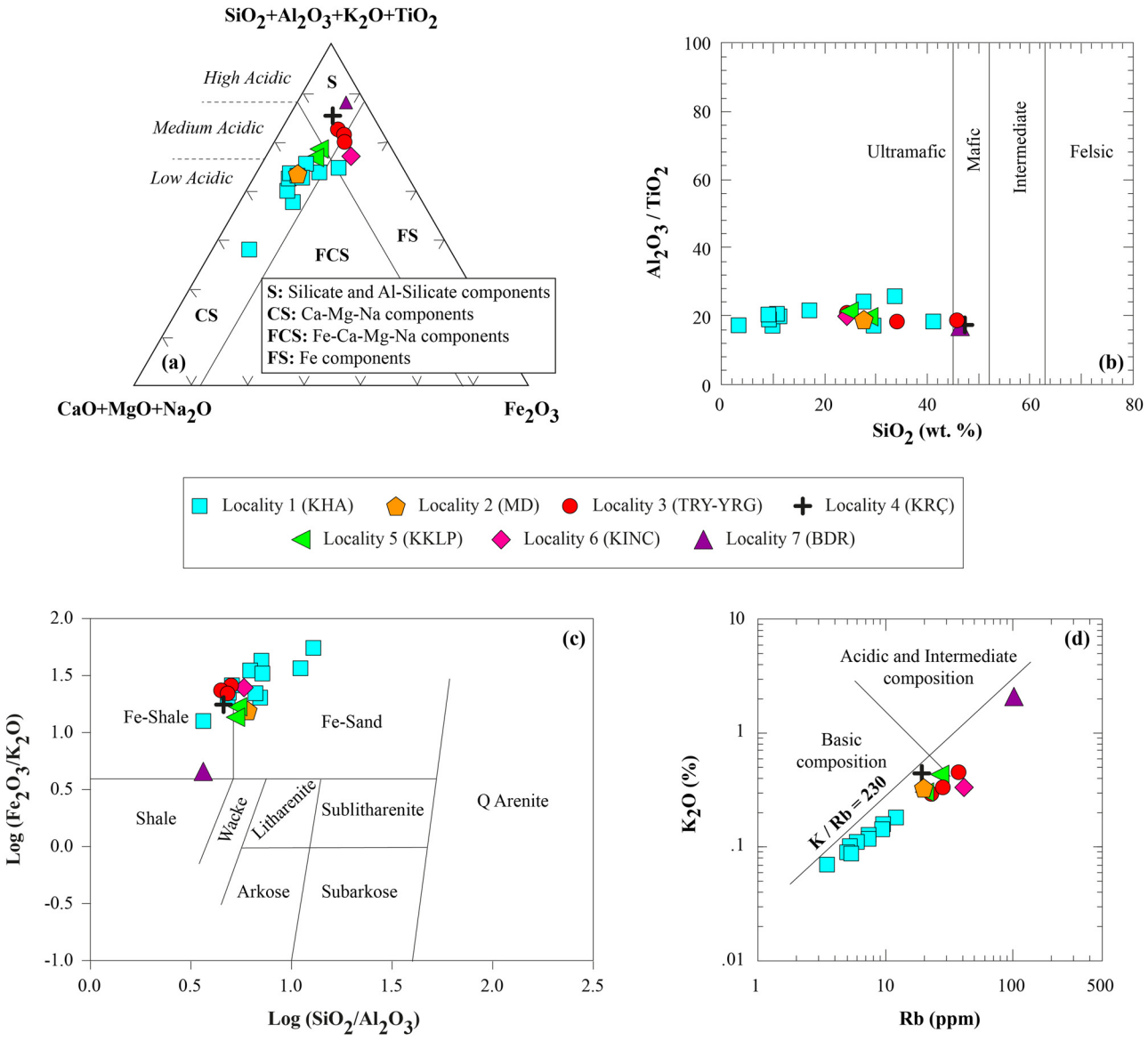

Figure 7: Classification of inorganic/mineral constituents on (a) (SiO_2 + Al_2O_3 + K_2O + TiO_2)-(CaO + MgO + SO_3 + Na_2O)-(Fe_2O_3) triangular diagram [53], (b) (Al_2O_3/TiO_2) vs SiO_2(%) [54], (c) log(Fe_2O_3/K_2O) vs log (SiO_2/Al_2O_3) [55], and (d) K_2O(%) vs Rb (ppm) binary diagrams [56].

8 Provenance and depositional characteristics of carbonaceous rocks

The major oxide and trace element chemistry of sedimentary rocks is closely related to the lithology of the source area from which they are derived. While the major oxide elements are easily mobilized during the transportation and depositional processes, trace elements such as Ba, Nb, La, Th, Zr, Ni, Cr, Co, V, and Sc are relatively immobile. Therefore, trace elements are commonly utilized to define the source area characteristics of sedimentary rocks [57–60]. Ba, Nb, La, Zr, and Th elements are mostly concentrated in feldspar, biotite, amphibole, monazite, zircon, apatite, and sphene minerals, which are diagnostic of felsic rocks. On the other hand, Ni, Cr, Co, V, and Sc elements are very high concentrations in olivine, pyroxene, spinel, chromite, and rutile minerals which are characteristic components of mafic-ultramafic igneous rocks. The Hf vs La/Th, Co/Th vs La/Sc, and Th vs Sc diagrams are commonly utilized for provenance characteristics (Figure 8a–c). Average basalt, granite, and ultramafic rock compositions [50] are also included in these diagrams. Most of the carbonaceous rocks are chemically closer to that of mafic-ultramafic rock composition in

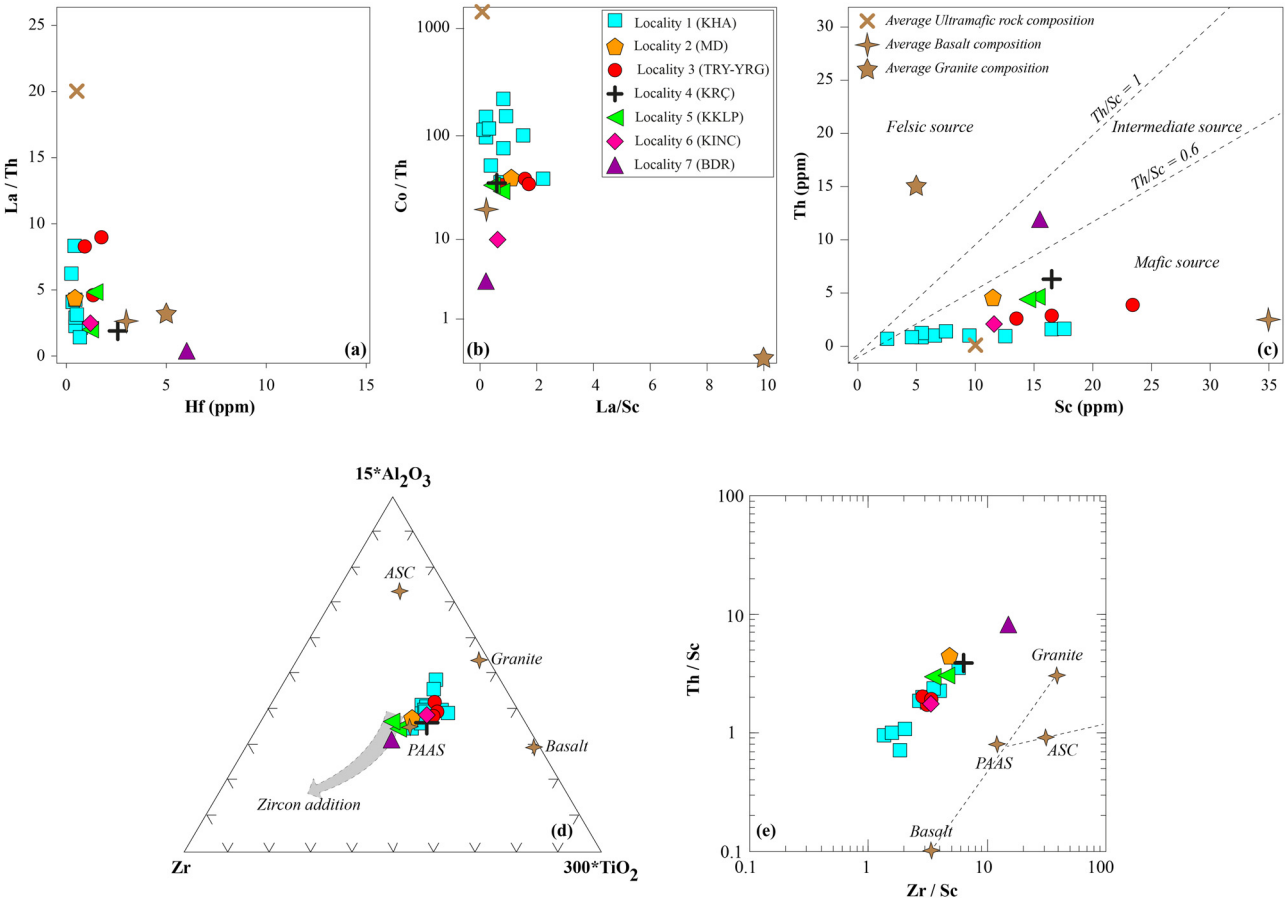

Figure 8: Chemical differentiation diagrams of carbonaceous rocks: (a) La/Th vs Hf diagram, (b) Co/Th vs La/Sc binary plot, (c) Th vs Sc diagram for provenance characteristics, (d) 15*Al_2O_3-Zr-300*TiO_2 ternary diagram, (e) Th/Sc vs Zr/Sc for sediment sorting and deposition rate.

these diagrams. Moreover, high Fe_2O_3, MgO, Cr, Co, and Ni contents of carbonaceous rocks are indicative of a significant contribution from mafic-ultramafic rocks in the source region. The Ni/Co, Cr/V, Cr/Th, Co/Th, Sc/Th, Ba/Nb, La/Th, La/Sc, Eu/Eu*, Ce/Ce*, and Pr/Pr* ratios are presented in Table 3. The average coal, NASC, PAAS, UCC, ASC, average granite, basalt, and ultramafic rock values are also given in Table 3 for comparison. Carbonaceous rocks are similar to average basalt/ultramafic rock values. It indicates that the dominant rock lithologies in the source area consist of mafic-ultramafic rocks.

Al, Ti, and Zr elements are relatively more stable than other elements during the weathering processes in the source area. A ternary diagram based on Al_2O_3, TiO_2, and Zr was proposed to monitor sediment sorting and deposition rate, ignoring the weathering effect in the source area [60,61]. While the TiO_2/Zr ratio shows a wide distribution in mature sediments (sandstone and shale), this value shows a very limited distribution for immature sediments. The carbonaceous rocks were clustered at the center of 15*Al_2O_3–Zr-300*TiO_2 ternary diagram. They also show a limited distribution in terms of TiO_2/Zr ratio, indicating poor sorting and rapid deposition (Figure 8d).

To evaluate the effect of sedimentary recycling of the studied carbonaceous rocks, Th/Sc vs Zr/Sc binary diagram can be utilized. In this diagram, positive trends indicate the compositional changes and no or minor sedimentary recycling in the source area, while flat to negative orientations indicate that the siliciclastic have continuously undergone sedimentary recycling [25,60,62,63]. The carbonaceous rocks were derived from mafic/ultramafic basement rocks and were deposited without sedimentary recycling in the source area. It can also be stated that limited compositional changes occur over time (Figure 8e).

Paleosalinity is an important indicator to decide the marine or terrestrial environment. The CaO/(Fe_2O_3 + CaO) ratio can give an idea about paleosalinity of the depositional environment. If the depositional environment is

Table 3: Calculated Ni/Co, Cr/V, Cr/Th, Co/Th, Sc/Th, Ba/Nb, La/Th, La/Sc, Eu/Eu*, Ce/Ce*, and Pr/Pr* ratios of carbonaceous rocks

	Ni/Co	Cr/V	Cr/Th	Co/Th	Sc/Th	Ba/Nb	La/Th	La/Sc	Eu/Eu*	Ce/Ce*	Pr/Pr*
The carbonaceous rocks	10.3–35.2	3.3–21.5	81.4–1695.3	2.7–202.2	1.3–13.3	5.8–23.3	0.2–8.9	0.1–2.2	0.2–0.3	3.3–4.3	0.16–0.19
Average coal [50]	2.0	0.5	10.0	5.0	2.5	125.0	5.0	2.0	0.8	3.7	0.20
NASC [48]	2.3	1.0	10.2	2.1	1.2	48.9	2.5	2.1	0.2	4.3	0.16
PAAS [47]	2.4	0.7	7.5	1.6	1.1	34.2	2.6	2.4	0.2	4.3	0.16
Upper continental crust [99]	2.7	1.0	8.8	1.7	1.3	52.0	3.0	2.2	0.2	4.2	0.16
Average shale composition [49]	2.6	0.7	7.5	1.6	1.1	52.7	3.6	3.3	0.2	4.0	0.17
Average granite [50]	1.3	0.1	0.7	0.3	0.3	33.3	3.3	10	0.2	4.4	0.14
Average basalt [50]	2.9	1	113.6	20.5	15.9	33.0	2.7	0.2	0.3	3.7	0.21
Average ultramafic rocks [50]	18.2	28.8	46,000	2,200	200	5.0	20.0	0.1	—	—	—

$Eu/Eu^* = Eu/(Sm^*Gd)^{0.5}$; $Ce/Ce^* = Ce/(La^*Pr)^{0.5}$; $Pr/Pr^* = 2^*Pr/(Ce + Nd)$.

fresh water (river, lake, etc.), Fe-phosphate minerals are formed, and if it is salt water (evaporitic lake, marine, etc.) Ca-phosphate minerals are precipitated [19]. The $CaO/(Fe_2O_3 + CaO)$ ratios of the carbonaceous rocks range from 0.04 to 0.59 (average 0.17), indicating that the depositional environment is weakly saline (brackish water). The Sr/Ba ratio can be utilized to judge the paleosalinity. Based on the Sr/Ba ratio, the paleosalinity conditions are separated into three categories. The Sr/Ba ratio < 0.5 represent freshwater (terrestrial) environment, 0.5 < Sr/Ba < 1 represents brackish water (transitional) environment, and Sr/Ba ratio > 1.0 represent salt water (marine) environment [21,26]. The Sr/Ba ratio of carbonaceous rocks is in the range between 0.20 and 4.35 (average 1.16). This shows brackish water in a terrestrial environment. This result is also compatible with field observations and XRD analysis.

8.1 Weathering in source rocks

Rocks and minerals are deteriorated by physical and chemical weathering. Significant changes in rock and/or mineral chemistry occur during weathering processes. Elements such as Na, Ca, K, Mg, Si, Al, and Fe in the rock and/or mineral change depending on the weathering degree. Some diagrams and weathering indices (provide numerical data regarding the weathering degree) have been developed by researchers to determine the weathering degree [64,65 and references therein]. A K_2O–Fe_2O_3–Al_2O_3 triangular diagram can be applied to determine the weathering degree in source area [56]. In the K_2O–Fe_2O_3–Al_2O_3 triangular diagram, carbonaceous rocks are clustered in an area close to the Fe_2O_3 corner, away from the residual clays and shale fields, which are indicators of intense weathering (Figure 9a). In addition, the carbonaceous rocks contain chlorite-type weathering products which indicates that the rocks in source area have not yet undergone intense weathering. The Th/U ratio is a significant parameter for monitoring weathering degrees of rocks. Due to the increase in the weathering degree, the U content decreases significantly, while the Th/U ratio increases [25,47,66]. The Th/U ratios of carbonaceous rocks ranges from 0.12 to 9.00 (average 3.15). In Th/U vs U diagram, most of the carbonaceous rocks (except a few samples) are clustered in the area below the PAAS (4.7) and UCC (3.9) values (Figure 9b). Low Th/U ratios suggest weathering processes are slightly effective in the source area. The K/Cs ratio is another indicator that is commonly used to assess weathering degree in the source area. Cs is accumulated in clay minerals throughout the weathering process. As weathering degree increases, the

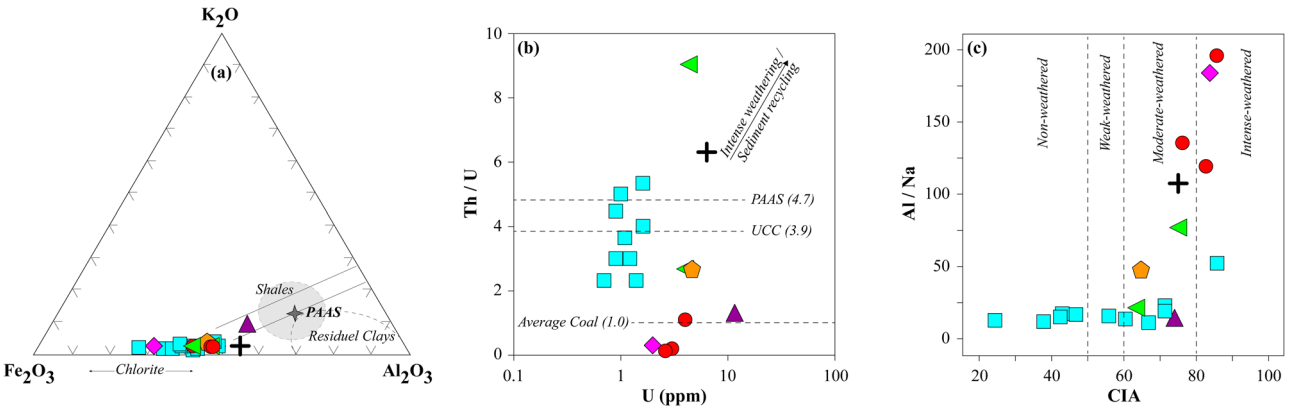

Figure 9: Diagrams for monitoring weathering degrees of carbonaceous rocks: (a) K_2O–Fe_2O_3–Al_2O_3 triangular diagram, (b) Th/U vs U binary diagram, and (c) Al/Na vs CIA binary diagram.

amount of clay minerals in the environment will increase, while the K/Cs ratio will decrease [67]. The K/Cs ratio of carbonaceous rocks are between 68.4 and 2646.9 (average 849.6). When the K/Cs ratio of carbonaceous rocks and PAAS value (2.048) are compared, weak to moderate weathering can be mentioned in the source area.

The chemical index of alteration (CIA) has been widely utilized as an indicator for determining weathering degree in rocks. The CIA was suggested by [64] for assessing the measure of the extent of conversion of feldspars to clay minerals such as kaolinite. The CIA values increase with increase in the clay minerals in the source rock. The CIA values of carbonaceous rocks range from 24.6 to 85.8 (average 63.3), indicating moderate weathering. In addition, most of the carbonaceous rocks fall in weak to moderately weathered regions except for a few samples which plot in the intense weathered field in Al/Na vs CIA diagram (Figure 9c). The Al/Na ratios of carbonaceous rocks (except for 5 samples) are similar and vary between 10.7 and 195.8 (average 53.7). The high Al/Na ratio could be caused by the diagenetic loss of Na^+ in that sample [17].

Significant information can be obtained about weathering degree in the source area and the maturation of sediments by calculating the index of compositional variability (ICV) [68,69]. ICV value is high in silicate minerals (biotite: 8; amphibole-pyroxene: 10–100; alkaline feldspar: 0.8–1; plagioclase: 0.6), whereas in minerals formed as a result of weathering (kaolinite: 0.03–0.05; montmorillonite: 0.15–0.3; illite-muscovite: 0.3) is low. ICV value >1 indicates that the rocks in source area have not yet undergone intense weathering [25,60]. ICV values in carbonaceous rocks vary between 1.26–8.60 (average 4.22), supporting weak to moderate weathering in the source area.

9 Paleoredox and paleoclimatic conditions

Some trace elements (such as Ni, V, Cr, U, Sr, Cu, Ga) and their ratios (such as Ni/Co, V/Cr, Sr/Cu, Ga/Rb, U/Th) in sedimentary rocks can be utilized to determine the paleoredox and paleoclimatic conditions since they are relatively immobile during depositional processes [18,20,23,25,31,47,70–73]. The V/(V + Ni) ratio is suited to define the oxidation state in the depositional environments. The V/(V + Ni) ratio <0.5 indicates an oxidizing environment, while the V/(V + Ni) ratio >0.5 indicates a reducing environment [74]. The V/(V + Ni) ratio of the carbonaceous rocks are variable, ranging from 0.02 to 0.25 (average 0.007). Low V/(V + Ni) ratios of carbonaceous rocks indicate oxidizing environment conditions during the sedimentation processes (Figure 10a). U/Th ratio is another parameter that reveals whether the depositional environment is oxic or anoxic. Based on the U/Th ratio, the paleoredox conditions are divided into three categories [70]. U/Th ratio <0.7 is considered as oxic condition; 0.7–1.2 dysoxic, and >1.25 anoxic. U/Th ratios of carbonaceous rocks range between 0.11 and 8.58 (average 1.16), reflecting the oxic conditions (Figure 10b). To avoid possible analytical errors of single element concentrations, Ce* has been used as an indicator of paleoredox conditions during the deposition of carbonaceous rocks. While high Ce* (>–0.1) is the most typical feature of oxic environments, Ce* (<–0.1) indicates anoxic environment, during the depositional processes [75]. The Ce* ranges between 0.06 and 0.96 (average 0.22), indicating oxic depositional environment (Figure 10c).

Suttner and Dutta [76] suggested SiO_2 vs (Al_2O_3 + K_2O + Na_2O) binary diagram to evaluate paleoclimatic condition during the accumulation of sedimentary rocks. The studied carbonaceous rock samples plot in the warm/

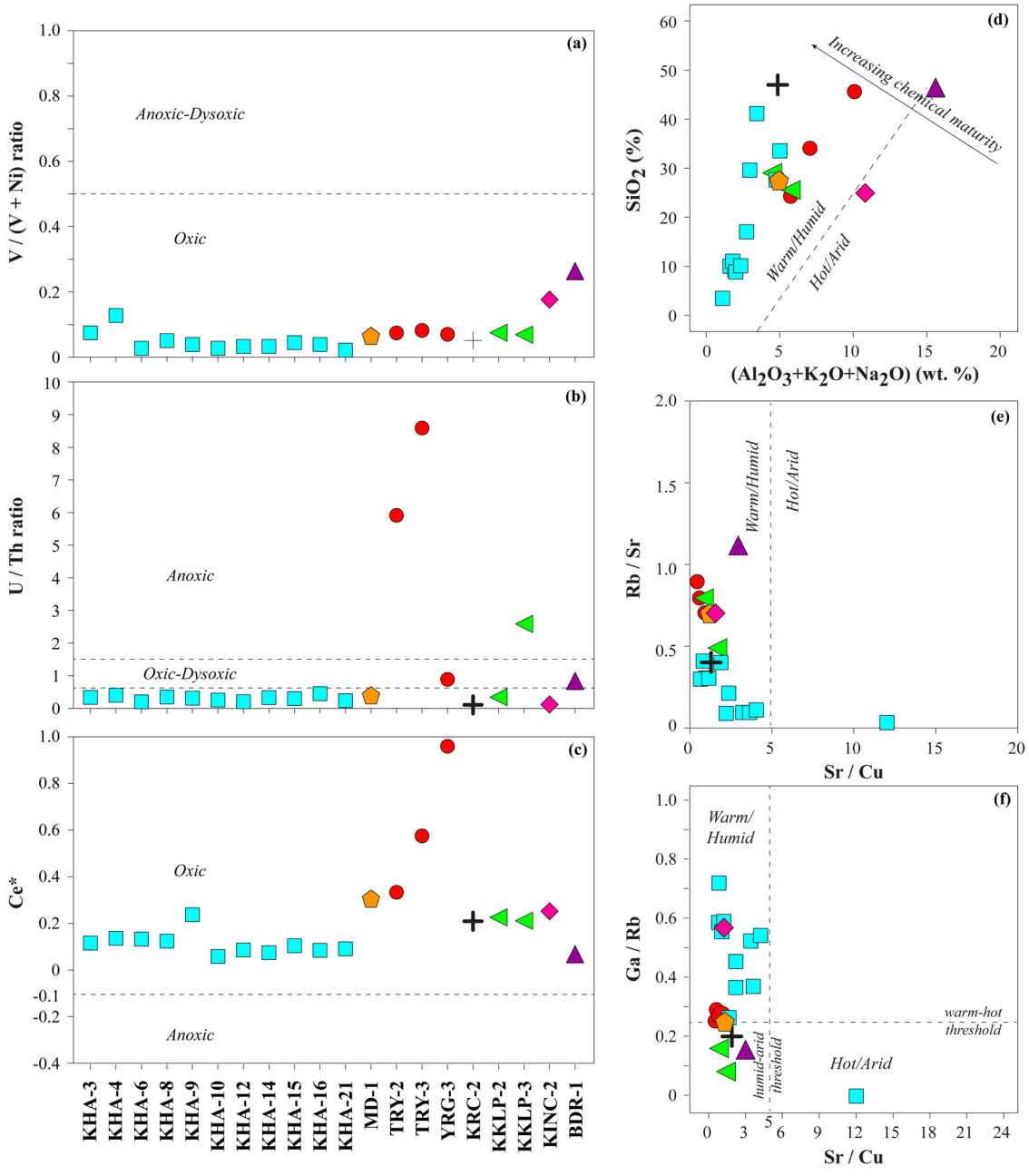

Figure 10: Paleoredox and paleoclimate conditions assessment diagrams of carbonaceous rocks.

humid field on SiO_2 vs (Al_2O_3 + K_2O + Na_2O) diagram (Figure 10d). The Rb/Sr, Ga/Rb, and Sr/Cu ratios of fine-grained sedimentary rocks can be applied to get information about paleoclimatic conditions during sedimentation. Rb and Ga do not occur in mineral forms in the Earth's crust, but they are present in significant amounts in other minerals such as feldspar, mica, and clay. On the other hand, Rb and Ga elements become enriched and adsorbed in clay minerals (illite, kaolinite, etc.) during weathering processes. Rocks in humid and rainfall regions decompose much faster than rocks in hot and dry regions. High Rb/Sr, Ga/Rb, and low Sr/Cu contents indicate warm and humid climatic conditions, while low Rb/Sr, Ga/Rb, and high Sr/Cu ratios indicate hot and arid climatic conditions [18,24,25,27]. The Rb/Sr, Ga/Rb, and Sr/Cu ratios of carbonaceous rocks range from 0.04 to 1.13 (average 0.45), 0.08 to 0.72 (average 0.36), and 0.49 to 11.97 (average 2.28), respectively, reflect the warm/humid climate condition during the sedimentation processes (Figure 10e and f).

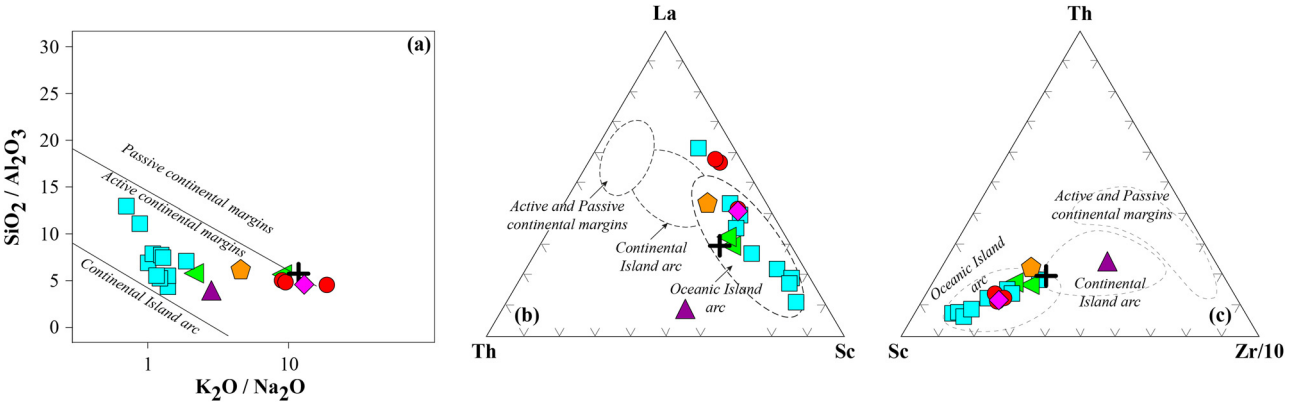

Figure 11: Tectonic discrimination for carbonaceous rocks: (a) SiO_2/Al_2O_3 vs K_2O/Na_2O, (b) La-Th-Sc, and (c) Th-Sc-Zr/10 diagrams.

10 Tectonic setting

While the behavior of major oxide elements gives little information about the tectonic setting of rocks, trace elements such as Sc, Ti, Co, Zr, La, and Th are widely used by many researchers because of immobility during alteration, metamorphism, and sedimentation processes [16,23,25,62,60,77–79]. While the SiO_2/Al_2O_3 ratios of carbonaceous rocks are in the range between 3.65 and 13.01 (average 6.08), the K_2O/Na_2O ratios vary between 0.52 and 16.50 (average 4.69). These values indicate that they were formed in an active margin environment on the SiO_2/Al_2O_3 vs K_2O/Na_2O diagram (Figure 11a). The La-Th-Sc and Th-Sc-Zr/10 discrimination diagrams recommended by Bhatia and Crook [80] are commonly utilized for the determination of the tectonic background of sedimentary rocks. The carbonaceous rocks mostly fall within the oceanic island arc field in these diagrams (Figure 11b and c).

11 Depositional environment

Depositional environments can be varied ranging from terrestrial (alluvial, lake, swamp, desert, etc.) to marine and transitional (delta, barrier-coastal, lakes-lagoons, etc.) environments. In all depositional environments, erosion, transportation, and deposition processes develop simultaneously both spatially and temporally. Most of the deposition models proposed for carbonaceous rocks suggest that carbonaceous rocks form in swamps on coastal deltas, alluvial plains, and lake-lagoon areas. As is known, the swamps are low-lying tracts of land which are periodically inundated by water [1,81–83]. Acıpayam-Çameli basin, in which the study area is located, is one of the tectonically active basins formed during the Neotectonic period in western Anatolia. It was filled by Oligocene-Upper Pliocene sedimentary rock units which are derived from the terrestrial environment (alluvial fan, braided and meandering stream, lacustrine) [37,38,84,85 and the references therein]. Following the opening of the Acıpayam-Çameli basin, the Oligocene-aged Bayıralan formation first started to fill the basin. Bayıralan formation was deposited in the transitional environment (coastal-shallow marine) according to the fossil contents in its sandstone-claystone levels and coral fauna in reef levels. In addition, thin carbonaceous rock layers with limited lateral and vertical distribution are also observed in the Bayıralan formation. Later, the middle-upper Miocene aged Kızılburun formation accumulated in the basin. Kızılburun formation starts with alluvial fan deposits at the bottom, continues with braided fluvial deposits at the upper levels, and ends with shallow lake sediments. The middle-upper Pliocene aged Yatağan formation consists of siliciclastic and carbonate rock units that alternate and show lateral transition with each other. Carbonaceous rocks are observed in both lithologies of the Yatağan formation. The Yatağan formation was deposited in a stream-shallow lake transition environment. It has been evaluated that the terrestrial plants and siliciclastic sediments, which are carried from the high areas to the plains of the basin by the rivers, are accumulated in the swamp environments near the river-lake coast, and then formed in an oxic environment where hot/humid climatic conditions are effective (Figure 12). The proposed deposition model is also compatible with organic petrography, gas chromatography (GC, GC-MS), biomarker, and carbon-oxygen isotope results given in ref. [15,41,86,87].

12 Heavy metal concentrations of carbonaceous rocks

The rapidly increasing social and economic requirements on the world scale have brought more energy production.

This situation has led to an increase in the demand for energy raw materials originating from the earth. While increasing energy production causes an increase in environmental problems, it requires a detailed investigation of the geochemical properties of the energy raw materials used. Carbonaceous rocks are a significant raw material for generating energy in power plants, and the geochemical properties and production processes of the carbonaceous rocks can cause environmental pollution. In energy production, the determination of heavy metal concentrations of carbonaceous rocks is important for the planning of raw material and waste management processes. The term heavy metal describes any metallic chemical element that has a relatively high density (>5 g/cm^3) and is toxic or poisonous even at low concentrations. Heavy metals are naturally found in the rocks and minerals that make up the earth's crust, in the tissues of living organisms, and in the composition of various substances in the environments. Heavy metals classified as potentially toxic to life forms by organizations such as the World Health Organization and the Arctic Monitoring and Assessment Program include Fe, As, Cd, Co, Cu, Hg, Ni, Pb, Sb, Se, V, Zn, and their metalloids. These elements are minor components in rock-forming minerals [88]. The heavy metal pollution potential of rocks can be determined by calculating different indexes. For this purpose, enrichment factor (Ef) and geo-accumulation index (I_{geo}) are frequently utilized [29,89–95].

13 Enrichment factors

The Ef is one of the indicators that is commonly used to evaluate the presence and concentration of heavy metal contents in rock samples. The Ef is calculated from the following equation [95]:

$$\text{Enrichment factor(Ef)} = (\text{Metal/RE})_{\text{Sample}} / (\text{Metal/RE})_{\text{Background}},$$

where Metal is the concentration of the selected element, RE is the value of reference element. The average coal composition is considered as background value [50]. Aluminum is commonly used by researchers as RE in carbonaceous rocks consisting of fine-grained sediments (shale, clay) due to its stable structure in weathering processes and as one of the main components of clay minerals. The classification suggested by [29] was used in the interpretation of the calculated Ef values. According to Chen et al. classification scheme, Ef <1 indicates no enrichment, Ef = 1–3 is minor enrichment, Ef = 3–5 is moderate enrichment, Ef = 5–10 is moderately severe enrichment, Ef = 10–25 is severe enrichment, Ef = 25–50 is very severe enrichment, and Ef >50 is extremely severe enrichment. The Ef values of Ni and Cr are the highest among the heavy metals and they have extremely severe enrichment. The Ef values of Cr (average 53.1) are lower than Ni (average 133.2). While the average Ef value of the Co element is 12.9, indicating moderately severe enrichment, the Ef values of Fe and V elements are 3.9 and 3.3, respectively, indicating moderate enrichment. The average Ef values in Cu, Se, and Mo elements are 1.5, 1.4, and 1.3, respectively, and exhibit minimal enrichments. In addition, there are no enrichments in As, Cd, Hg, Pb, and Zn elements. The Ef values of As, Cd, Hg, Pb, and Zn elements in carbonaceous rocks were similar to those found in background concentrations. Al-normalized Ef values of carbonaceous rocks are illustrated in Figure 13. Extreme to moderately severe enrichments in Ni, Cr, Co, Fe, and V elements are not thought to be of anthropogenic

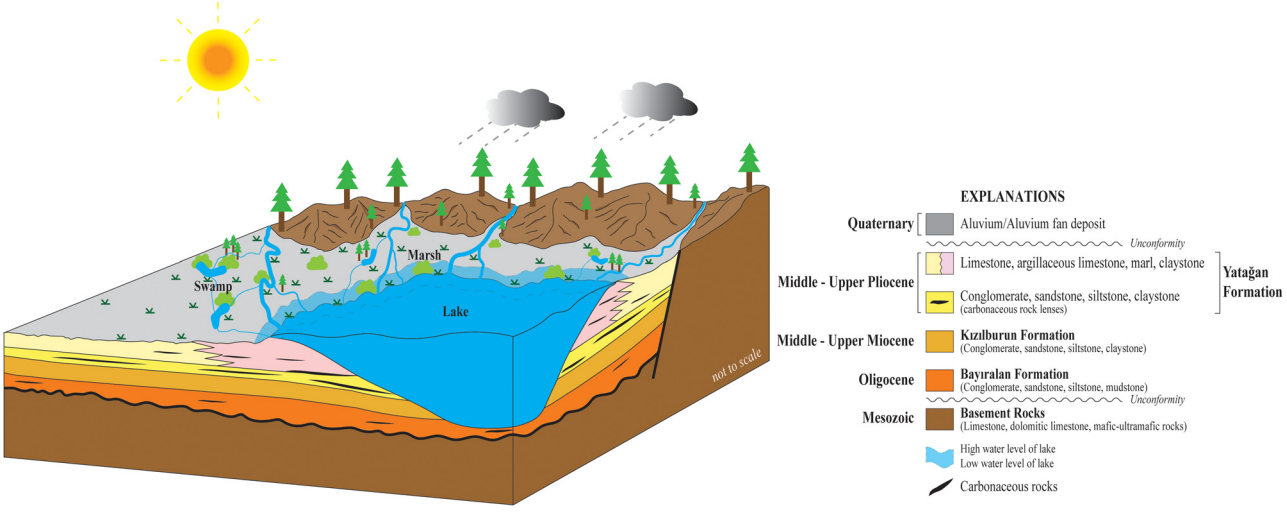

Figure 12: Model showing the depositional environment of the carbonaceous rocks (modified from [83]).

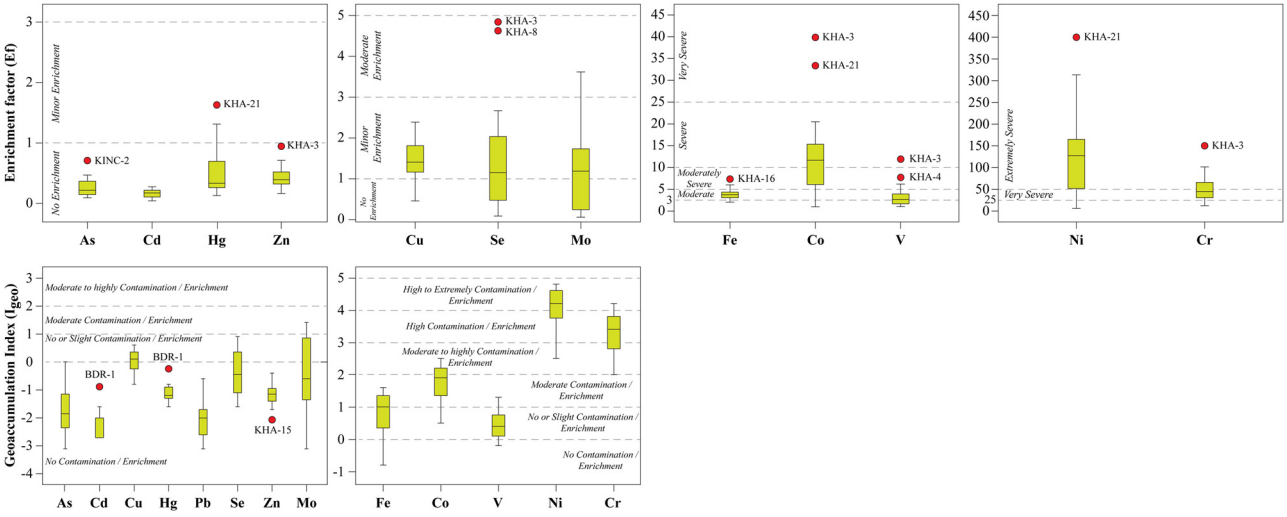

Figure 13: Boxplots showing Ef and I_{geo} of heavy metal contents in carbonaceous rocks.

origin. On the other hand, such enrichments are of lithological origin. With the presence of mafic/ultramafic basement rocks (Honaz Ophiolite and Karatepe Melange) in the source area, mineralogic and geochemical data indicate that such enrichments are of lithological origin. On the other hand, Efvalues between 0.5 and 1.5 (no enrichment to minor enrichment) indicate that the metal is entirely from background materials and natural processes.

14 Geoaccumulation index

Müller [96] proposed the geoaccumulation index (I_{geo}) to evaluate the current concentration of heavy metal elements in the sediment by comparing the current concentration with the geochemical background level. The I_{geo} for studied carbonaceous rocks was calculated using as the following equation:

$$\text{Geoaccumulation index } (I_{geo}) = \log_2(C_n/1.5{\star}B_n),$$

where C_n is the measured concentration of the heavy metal element in carbonaceous rocks, and B_n is the geochemical background value. The 1.5 is an empirical constant suggested to eliminate natural fluctuations that may occur due to lithology-induced effects and minimize their effects. The upper crust or average shale values suggested by different researchers are commonly used for geochemical background values. In this study, the average coal values [50] were utilized for geochemical background values [95,97,98]. Based on the Igeo values, the contamination/enrichment levels of elements are divided into six categories [95]. $I_{geo} \leq 0$ is considered as no contamination/no element enrichment; $0 < I_{geo} < 1$ is no or slight element enrichment, $1 < I_{geo} < 2$ is moderate element enrichment, $2 < I_{geo} < 3$ is moderate to high element enrichment, $3 < I_{geo} < 4$ is high element enrichment, $4 < I_{geo} < 5$ is high to extreme element enrichment, and $I_{geo} \geq 5$ values indicate extreme element enrichment. The average I_{geo} values of Ni (4.0) and Cr (3.3) exhibit high element enrichment among the 13 heavy metals studied. While the average I_{geo} value of the Co element is 1.8, pointing to moderate element enrichment, the average I_{geo} values of Fe and V elements are 0.8 and 0.5, respectively, implying slight element enrichment. On the other hand, the average I_{geo} values of As (−1.9), Cd (−2.3), Cu (−0.2), Hg (−1.3), Pb (−2.4), Se (−0.7), Zn (−1.4), and Mo (−0.8) elements show no element enrichment within the 13 heavy metals studied (Figure 13). The I_{geo} index results support the fact that the enrichments in Ni, Cr, Co, Fe, and V elements originate from the basement rock lithologies (Honaz Ophiolite and Karatepe Melange).

15 Conclusion

Field observations, mineralogical, organic, and inorganic geochemical properties of carbonaceous rocks in Pliocene siliciclastic rock sequence from the southeast of Denizli (SW Anatolia-Turkey) were characterized for the first time. Quantitative data were obtained to determine the characteristics of depositional environment with the results of elemental geochemistry. All findings and recommendations for future work can be summarized as follows.

i) Carbonaceous rocks among the siliciclastic layers of the Yatağan formation are observed as layered/laminated or lenticular-shaped with thicknesses varying between <3 and 15 cm. Based on organic chemical

investigations, TOC (%), T_{max} (°C), and HI values range from 3.01 to 43.80 wt% (average 22.42 wt%), 390 to 440°C (average 421°C), and 12–171 mg HC/g TOC (average 89 mg HC/g TOC), respectively. Carbonaceous rocks indicate good to excellent source rock potential and contain type III kerogen. Moreover, they have gas hydrocarbon potential, and their thermal maturity is an immature–early mature stage.

ii) Quartz, feldspar, pyrite, clay minerals (illite, smectite, kaolinite, and chlorite), and gypsum were identified as mineral matters in whole rock powdered XRD analyses of carbonaceous rocks. On the other hand, smectite, mixed-layer illite/smectite, kaolinite, and chlorite were determined as clay minerals in clay fraction XRD.

iii) Carbonaceous rocks exhibit close distribution in terms of CaO, NaO_2, and K_2O elements, whereas they display clear differences in terms of SiO_2, TiO_2, Al_2O_3, Fe_2O_3, and MgO elements. Although carbonaceous rocks have similar trace element concentrations, Ni (average 1956.9 ppm), Cr (average 934.3 ppm), Co (average 101.1 ppm), and V (average 107.5 ppm) elements are seen in remarkably high concentrations. This has been associated with detrital materials derived from mafic/ultramafic origins and transported to the depositional environment in different quantities.

iv) Major oxides, trace elements, and Ni/Co, Cr/V, Cr/Th, Co/Th, Sc/Th, Ba/Nb, La/Th, La/Sc, Eu/Eu*, Ce/Ce*, and Pr/Pr* ratios of carbonaceous rocks show similarities to mafic/ultramafic igneous rocks formed on the active continental margin.

v) In PAAS, NASC, and ASC normalized spider diagrams, carbonaceous rocks were depleted 5–80 times according to PAAS, NASC, and ASC values. Depletions in K_2O, Ba, Ta, Ce, and P_2O_5 elements are quite clear in these diagrams. In PAAS, NASC, and ASC normalized REE diagrams, carbonaceous rocks display nearly flat patterns ($(La/Lu)_{PAAS}$ = 0.25–0.97; $(La/Lu)_{NASC}$ = 0.32–1.26; $(La/Lu)_{ASC}$ = 0.21–0.84). In addition, carbonaceous rocks have slightly positive Europium (Eu/Eu*) anomalies ($(Eu/Eu^*)_{PAAS}$ = 0.88–1.37; $(Eu/Eu^*)_{NASC}$ = 0.90–1.40; $(Eu/Eu^*)_{ASC}$ = 0.88–1.37) indicating the abundance of plagioclase and mafic mineral phases.

vi) In the various chemical diagrams, carbonaceous rocks are composed of inorganic components that are mafic-ultramafic composition, detrital origin, and precipitated in a brackish water environment under oxic conditions. Carbonaceous rocks were rapidly stored without recycling in the deposition environment where hot/humid climatic conditions were effective. Besides, Th/U and K/Cs ratio, CIA (24.6–85.8 with an average of 63.3), and ICV (1.26–8.60 with an average of 4.22) values of carbonaceous rocks indicate that the rocks in the source area have not yet undergone intense weathering. On the other hand, more quantitative geochemical parameters such as organic carbon isotopes can also be used in later studies to investigate the sedimentation processes.

vii) In terms of heavy metal concentrations, carbonaceous rocks were enriched in Ni, Cr, Co, Fe, and V, respectively. Extreme to moderately severe enrichments in Ni, Cr, Co, Fe, and V elements are thought to be of lithological origin. If carbonaceous rocks are utilized for electricity generation in power plants, their wastes may have the potential to create environmental pollution. Furthermore, Ni, Co, and Cr can be enriched by using several beneficiation methods (flotation, magnetic separation, etc.) to obtain metal nickel, cobalt, and chromium.

Acknowledgments: The authors would like to extend their special thanks to the reviewers, whose helpful comments and constructive evaluation have significantly improved the quality of the paper.

Funding information: This study was financially supported by the Scientific and Technological Research Council of Turkey (TUBITAK, project number 114Y668).

Author contributions: This manuscript was prepared by Tamer Koralay and Demet Banu Koralay. Tamer KORALAY: literature review, fieldwork – sampling, sample preparation for inorganic geochemical analysis, drawing geochemical diagrams, evaluating elemental geochemical analysis results, and writing the manuscript. Demet Banu KORALAY: literature review, fieldwork – sampling, sample preparation for organic geochemical analysis, evaluating results, and writing the manuscript.

Conflict of interest: The authors declare that they have no known competing financial interests or personal relationships that could have appeared to influence the work reported in this paper.

Data availability statement: The raw/processed data required to reproduce these findings cannot be shared at this time as the data also forms part of an ongoing study.

References

[1] Tucker ME. Sedimentary petrology: An introduction to the origin of sedimentary rocks. USA: John Wiley & Sons; 2001.

[2] Finkelman RB. Trace and minor elements in coal. In: Engel MH, Macko SA, editors. Organic geochemistry. Topics in geobiology. Vol. 11. Boston: Plenum Press; 1993.
[3] Greensmith JT. Petrology of the sedimentary rocks. Unwin Hyman Ltd.: London; 1989.
[4] Littke R, Leythaeuser D, Rullkötter J, Baker DR. Keys to the depositional history of the posidonia shale (Toarcian) in the Hils Syncline, Northern Germany. Geol Soc Spec Publ. 1991;58(1):311–33.
[5] Gmur D, Kwiecińska BK. Facies analysis of coal seams from the Cracow Sandstone series of the upper Silesia Coal Basin, Poland. Int J Coal Geol. 2002;52(1–4):29–44.
[6] Fabiańska MJ, Kruszewska KK. Relationship between petrographic and geochemical characterisation of selected South African Coals. Int J Coal Geol. 2003;54(1–2):95–114.
[7] Petersen HI. The petroleum generation potential and effective oil window of humic coals related to coal composition and age. Int J Coal Geol. 2006;67(4):221–48.
[8] Korkmaz S, Kara-Gülbay R. Organic geochemical characteristics and depositional environments of the Jurassic coals in the Eastern Taurus of Southern Turkey. Int J Coal Geol. 2007;70(4):292–304.
[9] Sahay V. Limitation of petrographic indices in depositional environmental interpretation of coal deposits. Open Geosci. 2011;3(3):287–90.
[10] Hoş-Çebi F, Korkmaz S. Organic geochemistry and depositional environments of eocene coals in Northern Anatolia, Turkey. Fuel. 2013;113:481–96.
[11] Koralay DB. Organic geochemical and isotopic (C and N) characterization of carbonaceous rocks of the Denizli Area, Western Turkey. J Pet Sci Eng. 2014;116:90–102.
[12] Kara-Gülbay R. Organic geochemical and petrographical characteristics of coal bearing Oligo-Miocene sequence in the Oltu-Narman Basin (Erzurum), NE Turkey. Int J Coal Geol. 2015;149:93–107.
[13] Karayiğit Aİ, Littke R, Querol X, Jones T, Oskay RG, Christanis K. The Miocene coal seams in the Soma basin (W. Turkey): Insights from Coal petrography, mineralogy and geochemistry. Int J Coal Geol. 2017;173:110–28.
[14] Mastalerz M, Drobniak A, Stankiewicz AB. Origin, properties, and implications of solid bitumen in source-rock reservoirs: A review. Int J Coal Geol. 2018;195:14–36.
[15] Koralay DB. Paleoenvironmental Significance of Biomarker and Stable Isotope (^{2}H, ^{13}C, ^{15}N, ^{18}O, and ^{34}S) Investigations on a Pliocene Coal-Bearing Sequence (Denizli Basin, Southwestern Turkey). J Afr Earth Sci. 2020;171:103948.
[16] Bhatia MR. Plate tectonics and geochemical composition of sandstones. J Geol. 1983;91(6):611–27.
[17] Kasanzu C, Maboko MAH, Manya S. Geochemistry of fine-grained clastic sedimentary rocks of the neoproterozoic Ikorongo Group, NE Tanzania: Implications for provenance and source rock weathering. Precambr Res. 2008;164(3–4):201–13.
[18] Xu H, Liu B, Wu F. Spatial and temporal variations of Rb/Sr ratios of the bulk surface sediments in Lake Qinghai. Geochem Trans. 2010;11:3.
[19] Wang J, Yao W, Wang Q, Zhou J, Li J. Geochemistry of elements in the coal seams of the Xishanyao formation from Gashunwusan Mine, Xinjiang, Northwest China. Open Fuels Energy Sci J. 2016;9:11–20.
[20] Koralay DB. A review of the elemental composition and redox conditions of Oligocene organic matter-rich deposits, Western Anatolia, Turkey. J Eng Res Appl Sci. 2018;7(1):711–21.
[21] He C, Ji L, Su A, Wu Y, Zhang M, Zhou S, et al. Source-rock evaluation and depositional environment of black shales in the Triassic Yanchang Formation, Southern Ordos Basin, North-Central China. J Pet Sci Eng. 2019;173:899–911.
[22] Koralay DB, Koralay T. Geochemistry for the Pliocene Carbonaceous Rocks from Southeastern Denizli: Provenance Signature and Tectonic Setting. Proceeding of the International Multidisciplinary Scientific GeoConference-SGEM. 2019;19(1.1):211–9.
[23] Han S, Zhang Y, Huang J, Rui Y, Tang Z. Elemental geochemical characterization of sedimentary conditions and organic matter enrichment for Lower Cambrian shale formations in Northern Guizhou, South China. Minerals. 2020;10(9):793.
[24] Hou H, Liu S, Shao L, Li Y, Wang C. Elemental geochemistry of the Middle Jurassic shales in the northern Qaidam Basin, Northwestern China: Constraints for tectonics and paleoclimate. Open Geosci. 2021;13(1):1448–62.
[25] Mikheeva EA, Demonterova EI, Ivanov AV. Geochemistry of the Cheremkhovo and Lower Prisayan Formations from the Jurassic Irkutsk Coal-Bearing Basin: Evidence for Provenance and Climate Change in Pliensbachian-Toarcian. Minerals. 2021;11(4):357.
[26] Wang A, Wang Z, Liu J, Xu N, Li H. The Sr/Ba Ratio Response to Salinity in Clastic Sediments of the Yangtze River Delta. Chem Geol. 2021;559:119923.
[27] Zhou T, Zhou Y, Zhao H, Li M, Mu H. Depositional setting and enrichment mechanism of organic matter of Lower Cretaceous shale in Ri-Qing-Wei basin in the Central Sulu Orogenic Belt. Front Earth Sci. 2022;9:808916.
[28] Szczepanska J, Twardowska I. Distribution and environmental impact of coal-mining wastes in Upper Silesia, Poland. Env Geol. 1999;38(3):249–58.
[29] Chen CW, Kao CM, Chen CF, Dong CD. Distribution and accumulation of heavy metals in the sediments of Kaohsiung Harbor, Taiwan. Chemosphere. 2007;66(8):1431–40.
[30] Nowrouzi M, Pourkhabbaz A. Application of geoaccumulation index and enrichment factor for assessing metal contamination in the sediments of Hara Biosphere Reserve, Iran. Chem Speciat Bioavailab. 2014;26(2):99–105.
[31] Ding J, Zhang J, Tang X, Huo Z, Han S, Lang Y, et al. Elemental geochemical evidence for depositional conditions and organic matter enrichment of black rock series strata in an Inter-Platform Basin: The lower carboniferous Datang formation, Southern Guizhou, Southwest China. Minerals. 2018;8(11):509.
[32] Liu X, Bai Z, Shi H, Zhou W, Liu X. Heavy metal pollution of soils from coal mines in China. Nat Hazards. 2019;99(2):1163–77.
[33] Liu X, Jing M, Bai Z. Heavy metal concentrations of soil, rock, and coal gangue in the geological profile of a large open-pit coal mine in China. Sustainability. 2022;14(2):1020.
[34] Ercan T, Günay E, Baş H. Petrology and plate tectonic implications of Denizli Volcanics. Bull Geol Soc Turk. 1983;2:153–8 (in Turkish with English abstract).
[35] Sarıkaya H. Geological Map of the Denizli (M22-c2-c3-c4-d3). Mineral Res. Expl. Direct. Turkey (MTA), Ankara, Turkey: 1986.

[36] Okay AI. Geology of the Menderes Massif and the Lycian Nappes South of Denizli, Western Taurides. Bull Min Res Explor. 1989;109:37–51.
[37] Konak N, Akdeniz N, Çakır NH. Çal-Çivril-Karahallı Dolaylarının Jeolojisi, Mineral Res. Expl. Direct. Turkey (MTA), Ankara, Scientific Report No. 8949; 1990 (in Turkish).
[38] Sun S. Denizli-Uşak Arasının Jeolojisi ve Linyit Olanakları. Mineral Res. Expl. Direct. Turkey (MTA), Ankara, Scientific Report No. 9985; 1990 (in Turkish).
[39] Akbulut A, Kadir S. The geology and origin of sepiolite, palygorskite and Saponite in Neogene Lacustrine Sediments of the Serinhisar-Acipayam Basin, Denizli, SW Turkey. Clays Clay Min. 2003;51(3):279–92.
[40] Semiz B, Çoban H, Roden MF, Özpınar Y, Flower MF, McGregor H. Mineral composition in cognate inclusions in Late Miocene-Early Pliocene potassic lamprophyres with affinities to lamproites from the Denizli region, Western Anatolia, Turkey: Implications for Uppermost Mantle Processes in a Back-Arc Setting. Lithos. 2012;134:253–72.
[41] Koralay DB, Koralay T. Investigation of Geochemistry and Organic Petrographic Characteristics of Organic Matter-Rich Rocks from Southeast of Denizli (Honaz/SW Turkey), Technical Report for Scientific and Technological Research Council of Turkey, Ankara, Grant No. 114Y668; 2018 (in Turkish with English abstract).
[42] Tissot BP, Welte DH. From Kerogen to Petroleum. In: Tissot BP, Welte DH, editors. Petroleum formation and occurrence. Berlin, Heidelberg: Springer; 1984. p. 160–98.
[43] Peters KE. Guidelines for evaluating petroleum source rock using programmed pyrolysis. AAPG Bull. 1986;70(3):318–29.
[44] Langford FF, Blanc-Valleron MM. Interpreting Rock-Eval pyrolysis data using graphs of pyrolizable hydrocarbons vs total organic carbon. AAPG Bull. 1990;74(6):799–804.
[45] Hunt JM. Petroleum geochemistry and geology. 2nd edn. New York: WH Freeman and Company; 1996.
[46] Littke R. Deposition of organic matter-rich sediments. Berlin, Heidelberg: Springer; 1993.
[47] Taylor SR, McLennan SM. The continental crust: its composition and evolution. Blackwell: Oxford; 1985.
[48] Gromet LP, Dymek RF, Haskin LA, Korotev RL. The North American shale composite: Its compilation, major and trace element characteristics. Geochim Cosmochim Acta. 1984;48:2469–82.
[49] Li YH. A Compendium of geochemistry: From the solar Nebula to the human brain. Princeton: Princeton University Press; 2000.
[50] Reimann C, De Caritat P. Chemical elements in the environment: factsheets for the geochemist and environmental scientist. Springer Science & Business Media; 1998.
[51] MacRae ND, Nesbitt HW, Kronberg BI. Development of a positive Eu anomaly during diagenesis. Earth Planet Sci Lett. 1992;109(3–4):585–91.
[52] Vassilev SV, Vassileva CG, Baxter D, Andersen LK. Relationships between chemical and mineral composition of coal and their potential applications as genetic indicators. Part 1. chemical characteristics. Geol Balc. 2010;39(3):21–41.
[53] Vassilev SV, Vassileva CG. A new approach for the combined chemical and mineral classification of the inorganic matter in Coal. 1. chemical and mineral classification systems. Fuel. 2009;88(2):235–45.
[54] Le Bas MJ, Le Maitre RW, Streckeisen A, Zanettin B. A chemical classification of volcanic rocks based on the total alkali-silica diagram. J Pet. 1986;27:745–50.
[55] Herron MM. Geochemical classification of terrigenous sands and shales from core or log data. J Sediment Pet. 1988;58(5):820–9.
[56] Wronkiewicz DJ, Condie KC. Geochemistry and mineralogy of sediments from the Ventersdorp and Transvaal Supergroups, South Africa: Cratonic evolution during the early Proterozoic. Geochim Cosmochim Acta. 1990;54(2):343–54.
[57] McLennan SM, Taylor SR. Sedimentary rocks and crustal evolution: Tectonic setting and secular trends. J Geol. 1991;99(1):1–21.
[58] Cullers RL. The geochemistry of shales, siltstones and sandstones of pennsylvian-permian age, Colorado, USA: Implications for Provenance and Metamorphic Studies. Lithos. 2000;51:181–203.
[59] Roser BP, Cooper RA, Nathan S, Tulloch AJ. Reconnaissance sandstone geochemistry, provenance, and tectonic setting of the lower Paleozoic terranes of the West Coast and Nelson, New Zealand. N Z Geol Geophys. 1996;39(1):1–16.
[60] Caracciolo L, Le Pera E, Muto F, Perri F. Sandstone petrology and mudstone geochemistry of the peruc-korycany formation (Bohemian Cretaceous Basin, Czech Republic). Int Geol Rev. 2011;53(9):1003–31.
[61] Garcia D, Coehlo J, Perrin M. Fractionation between TiO_2 and Zr as a measure of sorting within shale and sandstone series (Northern Portugal). Eur J Miner. 1991;3:401–14.
[62] McLennan SM, Hemming S, McDaniel DK, Hanson GN. Geochemical approaches to sedimentation, provenance, and tectonics. Geol Soc Am. 1993;284:21–40.
[63] Cullers RL. The controls on the major and trace element variation of shales, siltstones, and sandstones of Pennsylvanian-Permian age from uplifted continental blocks in Colorado to platform sediment in Kansas, USA. Geochim Cosmochim Acta. 1994;58(22):4955–72.
[64] Koralay T, Çelik SB. Minero-petrographical, physical, and mechanical properties of moderately welded ignimbrite as a traditional building stone from Uşak Region (SW Turkey). Arab J Geosci. 2019;12(23):1–17.
[65] Ferdous F, Farazi AH. Geochemistry of tertiary sandstones from Southwest Sarawak, Malaysia: Implications for provenance and tectonic setting. Acta Geochim. 2016;35(3):294–308.
[66] Perri F, Critelli S, Cavalcante F, Mongelli G, Dominici R, Sonnino M, et al. Provenance signatures for the Miocene volcaniclastic succession of the Tufiti di Tusa Formation, Southern Apennines, Italy. Geol Mag. 2012;149(3):423–42.
[67] Nesbitt HW, Young GM. Early proterozoic climates and plate motions inferred from major element chemistry of lutites. Nature. 1982;299:715–7.
[68] Cox R, Lowe DR, Cullers RL. The influence of sediment recycling and basement composition on evolution of mudrock chemistry in the Southwestern United States. Geochim Cosmochim Acta. 1995;59(14):2919–40.
[69] Cox R, Lowe D. A conceptual review of regional-scale controls on the composition of clastic sediment and the co-evolution of continental blocks and their sedimentary cover. J Sediment Res. 1995;A65(1):1–12.
[70] Wignall PB, Myers KJ. Interpreting the benthic oxygen levels in mudrocks: A new approach. Geol. 1988;16:452–5.

[71] Jones B, Manning DA. Comparison of geochemical indices used for the interpretation of palaeoredox conditions in ancient mudstones. Chem Geol. 1994;111(1–4):111–29.
[72] Rimmer SM. Geochemical paleoredox indicators in Devonian-Mississippian black shales, central Appalachian Basin (USA). Chem Geol. 2004;206(3–4):373–91.
[73] El Aouidi S, Fakhi S, Laissaoui A, Malek OA, Benmansour M, Ayach A, et al. Geochemical characterization of the black shale from the Ama Fatma coastal site in the Southwest of Morocco. Am J Chem. 2017;7(5):153–62.
[74] Zuo X, Li C, Zhang J, Ma G, Chen P. Geochemical characteristics and depositional environment of the Shahejie Formation in the Binnan Oilfield, China. J Geophys Eng. 2020;17(3):539–51.
[75] Wright J, Schrader H, Holser WT. Paleoredox variations in ancient oceans recorded by rare earth elements in fossil apatite. Geochim Cosmochim Acta. 1987;51(3):631–44.
[76] Suttner LJ, Dutta PK. Alluvial sandstone composition and paleoclimate; I. framework mineralogy. J Sediment Res. 1986;56(3):329–45.
[77] Pearce JA. Role of the Sub-Continental Lithosphere in Magma Genesis at Active Continental Margins. In: Hawkesworth CJ, Norry MJ, editors. Continental Basalts and Mantle Xenoliths, Shiva, Nantwich; 1983. p. 231–49
[78] Wilson M, Igneous, Petrogenesis A. Global tectonic approach. London: Harper Collins; 1989.
[79] Rollinson H. Using geochemical data. Essex, UK: Longman Scientific & Technical; 1993.
[80] Bhatia MR, Crook KA. Trace element characteristics of graywackes and tectonic setting discrimination of sedimentary basins. Contrib Miner Pet. 1986;92(2):181–93.
[81] McCabe PJ. Depositional environments of coal and coal-bearing strata. Sedimentology of coal and coal-bearing sequences; 1985. p. 11–42.
[82] Diessel CFK. Coal-bearing depositional systems. Berlin-Heidelberg: Springer-Verlag; 1992.
[83] Dai S, Bechtel A, Eble CF, Flores RM, French D, Graham IT, et al. Recognition of peat depositional environments in coal: A review. Int J Coal Geol. 2020;219:103383.
[84] Elitez İ, Yaltırak C, Sunal G. A new chronostratigraphy (^{40}Ar-^{39}Ar and U-Pb dating) for the middle section of the Burdur-Fethiye Shear Zone, SW Turkey (eastern Mediterranean). Turk J Earth Sci. 2018;27(5):405–20.
[85] Alçiçek MC, Mayda S, ten Veen JH, Boulton SJ, Neubauer TA, Alçiçek H, et al. Reconciling the stratigraphy and depositional history of the Lycian Orogen-top basins, SW Anatolia. Palaeobiodiverse Palaeoenviron. 2019;99(4):551–70.
[86] Koralay DB. Geç Miyosen Yaşlı Honaz (Denizli) Kömürlü Birimlerinin Organik Jeokimyasal Özellikleri ve Çökelme Ortamı. Pamukkale Univ J Eng Sci (PAJES). 2018;24(6):1192–9.
[87] Koralay DB. Deposition characteristics of pliocene coals in the Denizli region (SW Turkey) via organic petrography, geochemistry, and stable isotope composition. J Nat Gas Eng. 2020;84:103619.
[88] Siegel FR. Environmental geochemistry of potentially toxic metals. Vol. 32. Berlin: Springer; 2002.
[89] Taylor SR. Abundance of chemical elements in the continental crust: A new table. Geochim Cosmochim Acta. 1964;28:1273–85.
[90] Zoller WH, Gladney ES, Duce RA. Atmospheric concentrations and sources of trace metals at the South Pole. Science. 1974;83(4121):198–200.
[91] Hakanson L. An ecological risk index for aquatic pollution control. A sedimentological approach. Water Res. 1980;14(8):975–1001.
[92] Sutherland R. Bed sediment-associated trace metals in an urban stream, Oahu, Hawaii. Env Geol. 2000;39:611–27.
[93] Praveena SM, Ahmed A, Radojevic M, Abdullah MH, Aris AZ. Heavy metals in mangrove surface sediment of Mengkabong Lagoon, Sabah: Multivariate and geo-accumulation index approaches. Int J Environ Res. 2008;2(2):139–48.
[94] Ghrefat HA, Abu-Rukah Y, Rosen MA. Application of geoaccumulation index and enrichment factor for assessing metal contamination in the sediments of Kafrain Dam, Jordan. Env Monit Assess. 2011;178(1):95–109.
[95] Barbieri M. The importance of enrichment factor (EF) and geoaccumulation index (Igeo) to evaluate the soil contamination. J Geol Geophys. 2016;5(1):1–4.
[96] Müller G. Index of geoaccumulation in sediments of the Rhine River. Geol J. 1969;2:108–18.
[97] Yaqin JI, Yinchang F, Jianhui WU, Tan Z, Zhipeng B, Chiqing D. Using geoaccumulation index to study source profiles of soil dust in China. J Env Sci. 2008;20:571–8.
[98] Horasan BY. The environmental impact of the abandoned mercury mines on the settlement and agricultural lands; Ladik (Konya, Turkey). Env Earth Sci. 2020;79(10):1–13.
[99] Rudnic RL, Gao S. Composition of the continental crust. In: Rudnic RL, editor. Treatise on geochemistry, The crust. Netherlands: Elsevier Pergamon; 2004.